PCBM derivatives and copolymer blends for organic photovoltaic devices:

Computational modeling and analysis

Rodrigo Pérez-García

A thesis submitted in

fulfillment of the requirement for the award of the

Degree of Master of Chemistry (MSc)

European master in Theoretical Chemistry and Computational Modelling

Zernike Institute for Advanced Materials
Rijksuniversiteit Groningen

DECEMBER 2012

I hereby declare that this thesis entitled "PCBM derivatives and copolymer blends for organic photovoltaic devices (OPV): Computational modeling and analysis" is the result of my own research except as cited in the references. This thesis has not been accepted for any degree and is not concurrently submitted in candidature of any other degree.

Signature : 

Student : Rodrigo Pérez-García

Date : December 18th, 2012

Supervisors : Prof. Ria Broer and Dr. Remco W. A. Havenith (RuG)

Prof. Keiji Morokuma and Dr. Haibei Li (Kyoto Univ.)

Prof. Antonio Laganà (University of Perugia)

To my mentors

nani gigantum humeris insidentes

Acknowledgment

After almost two and a half years, this master program is finished eventually. These exciting years of study in Groningen, Perugia and Kyoto Universities make me not only possess a solid background in my major, but also to be in contact with quite interesting environments and many different cultures and people. The great medieval philosopher St. Thomas Aquinas said "Quidquid recipitur ad modum recipientis recipitur" and in my opinion, the experiences are linked to the people I share my life with. There are many to thank for these wonderful experiences and I will try to be exhaustive. I beg your pardon in case I forget somebody.

I am extremely thankful to my academic mentors, Ria Broer, Keiji Morokuma, Haibei Li and Remco W. A. Havenith for their encouraging support, generous patience, and professional guidance, all I have accomplished would not be true without them.

I am specially grateful to Piet Th. van Duijnen, Petra Rudolf, Wim C. Nieuwpoort, Manuel Yañez, Stephan Irle and Alex H. de Vries for their kind attention and sympathetic response to all my concerns and doubts.

The financial support of this master was of paramount importance for me. I am indebted to the European Commission and all that it represents (Erasmus Mundus [FPA 2010-0147] and ICI-Interfaces programs).

Prof. Antonio Laganà was always friendly to me, thank you very much.

Thanks to all my friends and colleagues Adrián Fernández Ibáñez, Alberto Vicente Cuadrado, Alicia Burgos Álvarez, Ana Martín Sómer, Anneke Claus, Andrii Rudavskyi, Carla Diaz Juhl, Chiara Paris, Christos Kalogeropoulos, Dalibor Hršak, Dan Hawtree, Daniel Sethio, David Ferro Costas, Dumitru-Claudiu Sergentu, Elvira Martín Martín, Ena Tiesinga, Engel G. Vrieling, Fed-

erico Filomia, Francisco Fernández García-Prieto, Gerrit-Jan Linker, Giovanni Bistoni, Guillermo Santamaría Pampliega, Hanif Muhammed Khan, Henriet van Mil, Hilde de Gier, Jaakko J. Uusitalo, Johan Heijnen, Juan Pablo Sánchez Castillo, Kemel Arafet Cruz, Lalita Shaki, Levan Tseretelli, Lorenzino Vaccari, Luis Miguel Azofra Mesa, Maitreyi Robledo Relaño, Manuel N. Melo, Marco Camboni, Marcos Menéndez San Francisco, Marianna Manca, Melinda Gyenge, Miguel Ángel Mompeán García, Muammar El Khatib, Oscar Chung, Rafa García Meseguer, Rémi Maurice, Roberto Di Remigio, Rob Klooster, Roland de Mul, Rui Silva, Shehryar Khan, Travis Harris, Ulrich Mayer, Vera Thiemig, Wanda Andreoni, Werner Hofstra for your dear spark and all those pleasant times spent together.

A special "thank you" to those who spent their own free time to help edit and proofread this manuscript (R.W.A.H., R.B., G.B. & M.M.).

I am most grateful to my parents. They ceaselessly loved and helped me in every choice I have made. As I know, that they will be the happiest and the most proud parents when they see their son getting this degree, I dedicate this project to them. I would also like to thank the rest of my family for the support they provided me through out my entire life, and in particular I must acknowledge Caterina Benincasa; without their love, encouragement and friendship, I would not have even started this master.

Finally, special thanks to Ria and Remco again. Thank you for giving me the opportunity to come to this university and for your contagious and extensive encouragement to challenge myself in academia. In an ideal world there will be only professors like you.

Rodrigo Pérez-García, Groningen 2012

When you set out on your journey to Ithaca,
pray that the road is long,
full of adventure, full of knowledge. [...]
And if you find her poor, Ithaca has not deceived you.
Wise as you have become, with so much experience,
you must already have understood what Ithacas mean.

C.P. Cavafy, Collected Poems

Summary

Organic Photo Voltaic (OPV) devices have attracted much attention due to their profitable electronic and mechanical properties. However, the synthesis of high efficiency mixtures remains a challenge. Several calculations have been performed in order to increase the understanding of how the DFTB technique performs in modeling OPV components: Systems based on mixtures of a low band gap polymer, -in this research- poly(4,4-dihexyldithieno(3,2-b:2',3'-d)silole)-2,6-diyl-alt-(2,1,3-benzothiadiazole)-4,7-diyl), (PSBTBT-6), and both [6,6]-phenyl C_{61}-butyric acid methyl ester, (PCBM), and its derivate [6,6]-phenyl-C_{61}-butyric acid (2-N,N-dimethylaniline-5-nitro)benzyl ester, (PCBPP).

In order to successfully equilibrate and get relevant configurations of the systems, molecular dynamic (MD) simulations are used. DFTB quantum mechanical theory was embraced to perform the MD and the subsequent solid state calculations. From the former, it was possible to select a broad range of snapshots to statistically investigate some electronic properties (i.e., Density Of States (DOS), charge differences, molecular orbitals).

The presented results suggest that SCC-DFTB is a computationally feasible and reliable method for modeling structure evolution and the properties of such a systems, comparable in accuracy with medium size basis set DFT calculations at the computational cost of standard semi-empirical methods.

In conclusion, the presented work-flow will serve to generate with high accuracy initial structures for subsequent calculations. These will evaluate further how likely the substitution constituents would lead to an increase of charge transfer from the copolymer to the fullerene derivative.

Riepilogo

I dispositivi Fotovoltaici Organici (OPV) hanno attratto molta attenzione per le loro vantaggiose proprietà elettroniche e meccaniche. Tuttavia, la sintesi di miscele caratterizzate da alta efficienza rimane una sfida ancora aperta. Sono stati effettuati numerosi calcoli allo scopo di ottenere una migliore comprensione circa l'impiego della tecnica DFTB nella modellizzazione di sistemi OPV basati su miscele di polimeri a basso bandgap - in questo studio - poly(4,4dihexyldithieno(3,2-b:2',3'-d)silole)-2,6-diyl-alt-(2,1,3-benzothiadiazole)-4,7-diyl), (PSBTBT-6), e sia [6,6]-phenyl C61-butyric acid methyl ester, (PCBM), che il suo derivato [6,6]-phenyl-C61-butyric acid (2-N,N-dimethylaniline-5-nitro)benzyl ester, (PCBPP).

Per poter equilibrare con successo e ottenere rilevanti configurazioni dei sistemi, sono state effettuate simulazioni di dinamica molecolare (MD). Inoltre la teoria quanto-meccanica DFTB è stata impiegata per effettuare la MD e i successivi calcoli di stato solido. Dalla teoria DFTB è stato possibile ricavare un ampio spettro di immagini allo scopo di investigare statisticamente alcune proprietà, come la Densità degli Stati (DOS) e le differenze di carica su formazioni complesse.

I risultati presentati suggeriscono che SCC-DFTB è un metodo computazionale praticabile e in grado di fornire risultati attendibili per lo studio delle proprietà delle strutture oggetto di studio, comparabile in quanto ad accuratezza ai calcoli DFT, con il costo computazionale di un metodo semi-empirico standard.

In conclusione, seguire la traccia del presente lavoro porterebbe servire per generare conformazioni che includano effetti elettronici, da usare come punto di partenza per lo studio del trasferimento di carica dal copolimero a diversi derivati del fullerene.

Contents

References 41

List of Figures

List of Tables

List of Appendices

Chapter 1

Introduction

In this chapter are discussed some theoretical aspects needed for the performed calculations as well as for establishing the research questions.

Le savant n'étudie pas la nature parce que cela est utile;
il l'étudie parce qu'il y prend plaisir,
et il y prend plaisir parce qu'elle est belle.
Henri Poincaré

1.1 Background

Energy is central when addressing the major challenges of the 21st century [1], challenges like climate change, sustainable economic and social development, human well-being, and global security. It has been projected that by 2050 worldwide energy consumption will increase to approximately 28 TW, from its 2006 level of around 11 TW. Looking at the data available, it is possible to assure that fossil fuels resources are enough to cope with the expected energy demand in the middle of the 21st century and beyond, according to an adequate management of the various forms of energy storage, coal, oil and gas [2]. Nevertheless the use of fossil energy reservoirs will result in an increase of the atmospheric CO_2 concentration. The actual political considerations to move the world's energy consumption towards a carbon-free situation, leads to a detriment of fossil fuels use [3, 4]. Renewable energy is perceived as a sustainable solution to ensure future energy supply, as well as being carbon dioxide emissions free or, at least, neutral.

Global consumption	**Hydro**	**Geothermal**	**Wind**	**Solar** (*albedo)
15 TW	7.2 TW	32 TW	870 TW	1.76 x10^5TW

Table 1.1: Energy available for harvesting from different sources compared to the global energy demand per year[1]

Solar energy is by far the renewable energy source with the greatest potential [2] (see Table 1.1) assuring a minimal environmental impact [5, 6]. It has the ability to cover the world's energy demand several thousand times over and, unlike fossil fuels, solar energy is readily available world-wide [7].

Organic photovoltaic devices (OPV) do not only seem to be the most viable choice to meet our clean energy demand but it will also help in the development of decentralized energy (off-grid) zones. Electrification based on the easy installation of light in rural households or the setting up of mini-grids (where OPV might be combined with other energy technologies) will enable the provision of key services such as education, security, communication and health [8]. Unfortunately, utilization of solar energy is still not so widely spread. It is a common believe that this is mainly so because it is not directly economically profitable. Current silicon based solar cells on the market, based on inorganic solid-state junction devices, are environmentally clean, but generally cumbersome and pretty expensive [9, 10], due to large amounts of materials required for production and the necessary purification levels. Though silicon cells have relatively high reported power conversion efficiencies (PCE) of between 18% and 25%, the efficiencies achieved in laboratory studies are often not conveyed in commercially available applications, due to problems with scale up and the requirement of highly controlled conditions. Silicon-based cells have dominated the photovoltaic market for the last fifty years and much research is still made into enhancing the existing systems. However, single junction silicon cells have a theoretical maximum power conversion capacity of about 30% (at one sun) established by the Schokley-Quiesser[1] limit which may not help to reach good market benefits. Organic nanomaterials are on the other hand very much attractive as shown in Figure 1.1, due to the favorably small amount of material needed and the likely associated decrease in cost per Watt in addition to the specific properties of these materials, like tunable transparency, unnecessary direct light radiation [11] or flexibility.

Solar cells are essentially p-n junctions of a very particular type. The

[1]The limit places maximum solar conversion efficiency around 33.7% assuming a single p-n junction with a typical band gap for silicon. That is, of all the power contained in sunlight falling on a silicon solar cell only 33.7% of that could ever be turned into electricity.

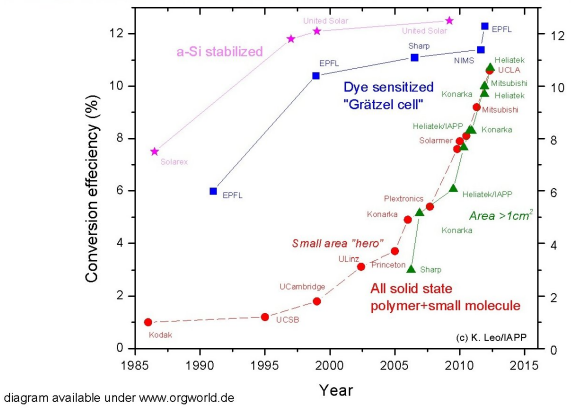

Figure 1.1: Development of OPV devices in the last years is high. As it is possible to see in the plot the 11% efficiency is at reach.

surface area in these devices should be big, as it has been shown to be a positive factor in the PCE of the cells [12]. In the photovoltaic cell, the theory explaining conversion of solar energy directly into electricity is the photoelectric effect (cf. Figure 1.2), first observed by the French scientist Becquerel in 1839, evolved with

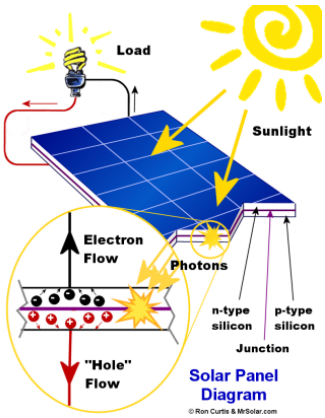

Figure 1.2: A solar cell is a kind of semiconductor device that takes advantage of the photovoltaic effect, in which electricity is produced when the semiconductor's PN junction is irradiated. The absorbed light excites the bound electrons into a higher energy state, making them free electrons. These free electrons move about in all directions within the crystal, leaving holes where the electrons used to be, and the holes also shift around the crystal.

the help of many scientists and then heuristically evaluated using a mathematical formulation by Einstein in the early years of the 20th century. Although much is already known there are still many challenges to overcome, mainly in the "recently" discovered organic cells.

There are many OPV cells' aspects that can be further improved to increase the PCE. Doing so hinges upon an understanding of the device physics and

the development of novel device architectures that overcome the other shortcomings inherent to organic devices (i.e. durability, processability, etc). The physical processes of well performing and cost-effective organic photovoltaic devices are paramount [5] if we want to achieve sustainable human development.

If the goal of reliably predicting properties from first principles via atomistic simulations, using intermolecular potentials [13] derived from quantum chemistry, could be turned into reality, many industries would profit, and clearly this would also be a major success of quantum statistical mechanics. However, this is not yet feasible and it is mandatory to do approximations and/or reduce the systems to handleable sizes.

A thorough theoretical assessment of the properties of these binary systems is important, but difficult due to the lack of availability of computer power for QM-MD simulations [14]. It is also important to bear in mind that obtaining appropriate results for the required time- and length scales of the systems is difficult using most available methods. The problem is even more complicated when one of the components is polymeric because additional factors such as molecular packing, chain-flexibility and molecular weight need to be considered [15]. Classical MD models do not take into account all the details of the electronic structure at the quantum level and thus cannot accurately predict the influence of specific groups of atoms on the physical properties. However, in the last few years, atomic scale MD has been quite successful in exploring different phenomena occurring at pico- to nanosecond time scales [16, 17]. It is still necessary to look at this problems using a multi-scale approach. DFTB methodology is a combined (quantum mechanical/molecular mechanical)-based molecular dynamics sampling technique able to explore molecular conformational landscapes in explicit environments. A powerful link between electronic description and feasibility to handle large system's dynamics.

To be able to perform successful simulations on bulk heterojunction type of systems, there is the need of a platform which incorporates numerical algorithms and takes into account such effects as temperature coupling, pressure coupling and conservation of constraints. That is why several MD packages have been developed over the years. Although not purely a MD package, the program used to conduct the present study is called DFTB+ [18] that can deal with dynamics while electronic structure is still taken into account.

In the following sections, the basic physics underlying the operation of single heterojunction devices will be described.

1.2 Organic semiconductors

The studies of several groups in conductivity of different organic amalgams with metallic properties, although not fully metallic constituted, led to the first molecular material with metallic conductivity. The year was 1977. Hideki Shirakawa, Alan MacDiarmid, and Alan Heeger (winners of the 2000 Nobel Prize in Chemistry) published their discovery that upon reaction with iodine, polyacetylene exhibited electrical conductivity many orders of magnitude higher than the neutral unreacted film [19]. A salt of [the electron acceptor] tetracyano-p-quinodimethane (TCNQ) and tetrathiafulvalene [electron donor] (TTF), which acted as a metal along one wide temperature range, appeared not so long after that. After this salt, many other organic compounds have been discovered that showed similar properties. Considering the low density of the polymers and the high density of metals, comparing equal masses, we conclude that these doped organic amalgams far exceed the conductivity of metals.

The main asset in the use of polymers resides in the low manufacturing costs. Organic semiconductors can be synthesized by cheap dissolution procedures. The interesting properties of conductive polymers include: the possibility of modulating the electrical conductivity and the chemical composition. The key to this versatility, and much of the unique properties of this class of materials, comes from the energy difference between the $\pi-$band, which is the highest occupied molecular orbital (HOMO), and the π^*-band, which is the lowest unoccupied molecular orbital (LUMO) is generally in the range between 1.5 to 3 eV [20]. It means that a $\pi \rightarrow \pi*$ transition is possible, for example, upon photon absorption of visible light.

1.2.1 Double layer OPV

Three main types of OPV have been developed, that is, single layer OPV, double layer OPV, and heterojunction OPV [21]. The latter, which is a special type of bulk double layer, has proven to have a very good performance. The bulk heterojunction is presently the most widely used photoactive layer. The name bulk-heterojunction (BHJ) solar cell has been chosen, because the interface (heterojunction) between both components is all over the bulk (c.f. Figure 1.3), in contrast to the classical (bilayer-)heterojunction. As a result of the intimate mixing, the interface where charge transfer can occur has increased enormously. The exciton, created after the absorption of light, has to diffuse towards this interface

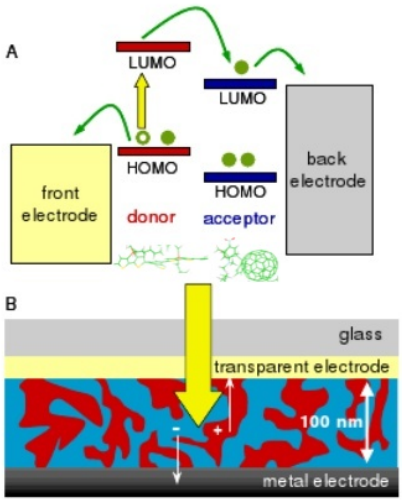

Figure 1.3: Schematic two-dimensional representation of a bulk-heterojunction structure. The common device structure is depicted here, with a intermixed photoactive layer sandwiched between a hole collecting transparent electrode (usually indium-doped tin oxide (ITO)) and an e- collecting electrode (typically metal, such as Al).

for charge generation to occur. The diffusion length of the exciton in organic materials, however, is typically 10 nm or less. This means that for efficient charge generation after absorption of light, each exciton has to find a donor-acceptor interface within a few nm, otherwise it will be lost and would not contribute to charge generation. An intimate bi-continuous network of donor and acceptor materials in the nanometer range should suppress exciton loss prior to charge generation, making BHJ very suitable as already announced.

Various combinations of donor and acceptor materials have been used to build bulk-heterojunction solar cells in which the composite active layer is inserted between two electrodes. One of the most promising combinations of materials is a blend of a low band gap copolymer as a donor and a fullerene, C_{60} derivative, as acceptor.

Whatever this mixture will be, the process of converting light energy into current could be summarized in five basic steps [22] as represented in Figure 1.4:

1. Photon absorption and excited state generation,
2. Diffusion of mobile excited states towards the interface,
3. Dissociation and subsequent charge separation states,

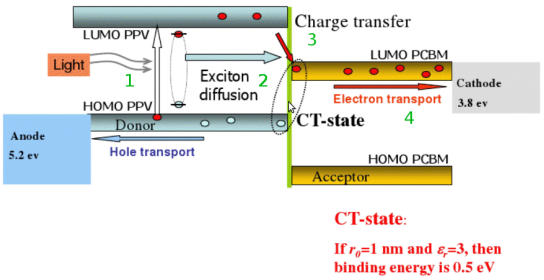

Figure 1.4: The basic operation of a OPV cell. The numbers refer to the processes explained in the text.

4. Charge migration and

5. Charge collection.

The basic operation of a single junction device described in more detail as a 5-step process is shown in Figure 1.5. The active layers of the device consist of a material with a low ionization potential, called the donor, and a material with a large electron affinity, called the acceptor. The total device active layer thickness is of the order of 100nm enabled by the high extinction coefficients of organic semiconductors. A thicker layer will provoke a huge charge recombination.

In a more detailed look, the conversion steps imply the following processes:

(1) The active layers absorb incident photons leading to the promotion of a molecule into an excited state. This is equivalent to the creation of an electron-hole pair in a conventional semiconductor. A major distinction with inorganic PV cells is that the excited state quickly (within ~10ps) relaxes to a bound state, called an exciton, that cannot be dissociated into a free electron and hole using electric fields typically present in devices [6]. The overall probability (or rate) of absorption can be given approximately by Fermi's Golden Rule,

$$P \propto \rho \mid \langle \psi_i \mid \hat{\mu} \mid \psi_f \rangle \mid^2 \tag{1.1}$$

where ψ_i and ψ_f are the initial and final electronic states, $\hat{\mu}$, the dipole operator (the perturbation on the system), and ρ is the density of final states in the material. This basic principle explains the absorption spectra of the semiconductors used to make solar cells.

(2) A fraction of the photogenerated excitons diffuse to the donor/acceptor (DA) interface before they decay radiatively or, more commonly, non-radiatively.

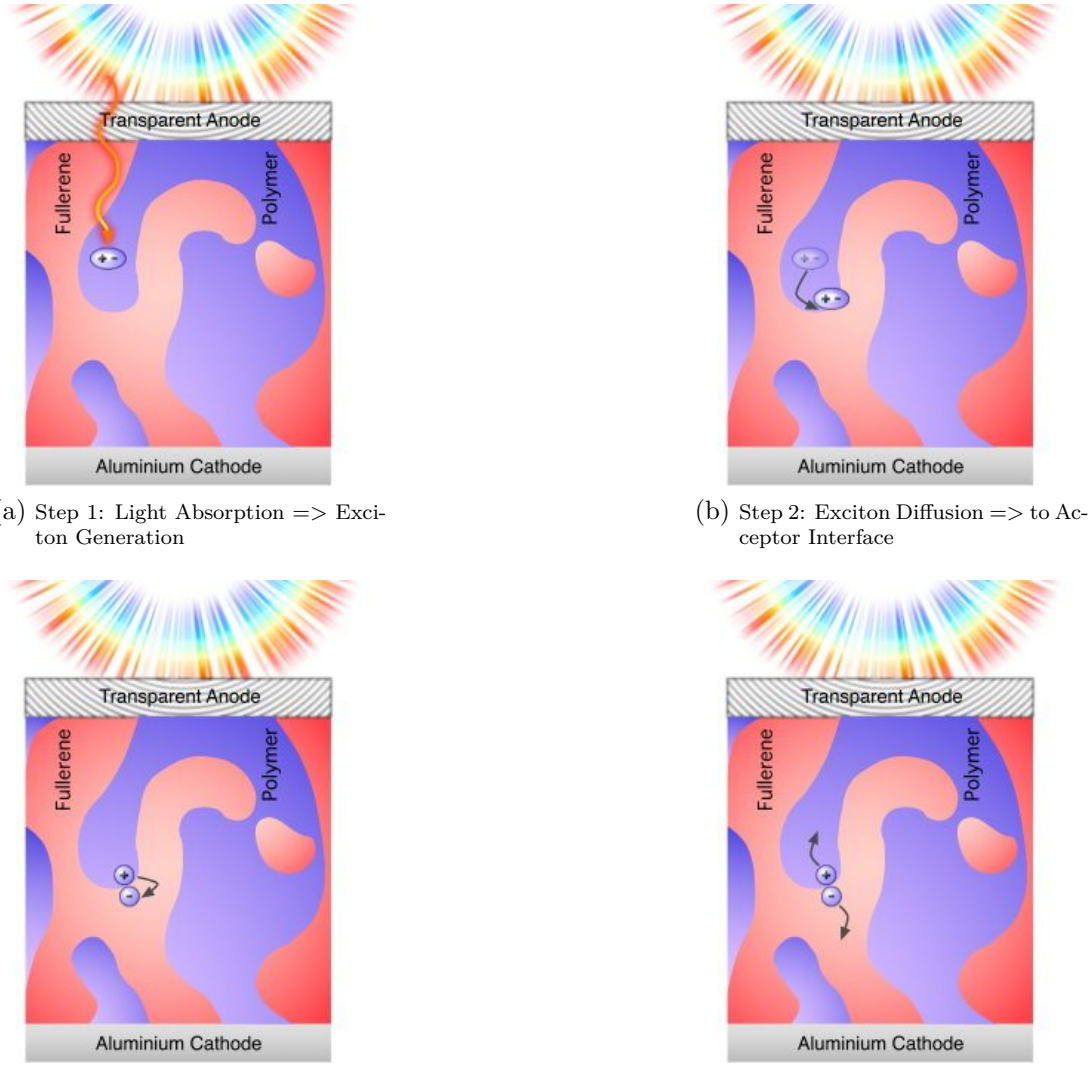

(a) Step 1: Light Absorption => Exciton Generation

(b) Step 2: Exciton Diffusion => to Acceptor Interface

(c) Step 3: Exciton Dissociation => Polaron Pair Generation

(d) Step 4: Polaron Pair Dissociation => Free Electron–Hole Pairs!

Figure 1.5: Operation of a OPV cell in more detail. (by Dr. Carsten Deibel)

(3) The bulk heterojunction architecture is an interpenetrating network of phases. Excitons residing on a donor (acceptor) molecule at the DA interface transfer an electron (hole) to an adjacent acceptor (donor) molecule. This charge-transfer step is usually exothermic and very fast (100 times faster than absorption). The result is an electron in the *lowest unoccupied molecular orbital* (LUMO) of an acceptor molecule and a hole in the *highest occupied molecular orbital* (HOMO) of a donor molecule. The electron-hole pair spans the DA interface and is referred to as a *geminate electron-hole pair* (GEHP). The spatial separation between the electron and hole immediately preceding the charge-transfer process is an important parameter that influences the next step [6].The LUMO_{donor}-$\mathrm{LUMO}_{acceptor}$ energy offset must be equal to or greater than the exciton binding energy.

(4) The GEHP is bound by a Coulomb attraction. Because of the presence of a barrier for both the electron and hole (they are each confined to a half space), diffusion of the electron and hole favors their separation. This is a driving force that is entirely statistical in nature. At the same time, an electric field may be present that aids or prevents GEHP dissociation. The loss of electron-hole pairs due to recombination of GEHPs is called *geminate recombination*. Exciton diffusion is the main efficiency bottleneck in planar bilayer organic PV cells. In bulk heterojunctions, DA junctions throughout active layers provide efficient exciton dissociation removing the exciton diffusion length bottleneck. An improved understanding of the physics underlying exciton diffusion length and the development of molecular materials with more appropriate exciton diffusion length are required [6, 23].

(5) In a final step, the charge carriers, now separated from their geminate partner, travel through the device structure and are collected at the electrodes if they do not recombine with an opposite carrier type en route. This type of recombination is called non-geminate since it involved electrons and holes that do not originate from the same exciton (different precursors states need to dissociate to generate free species which then find one other to recombine) and occur after the charges have been generated [6].

1.3 Molecular structures

A visual representations[2] of all the relevant structures for this work are presented below.

1.3.1 SBTBT-6

Typical copolymer subunits are shown in the Figure 1.6. Particularly, low band

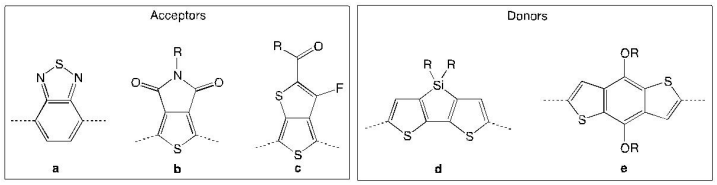

Figure 1.6: Typical donor acceptor constituents of the co-polymers used in OPV

[2]Generated using Visual Molecular Dynamics (VMD) software.[24]

gap semiconducting polymers containing silicon bridging heteroatoms have been the subject of much recent interest for organic photovoltaic cell (OPV) applications. Several studies have demonstrated that the electronic properties of the polymer backbone can be modified by interaction of the low lying $\pi*$ orbitals of the silicon atom with $\pi*$ orbitals of the conjugated system, primarily resulting in stabilization of the polymer LUMO in comparison to the carbon bridged analogues. Furthermore studies show that the introduction of electron- withdrawing benzothiadiazole molecules along the dithienosilole backbone further reduce the optical band gap and increase the interchain interaction [25].

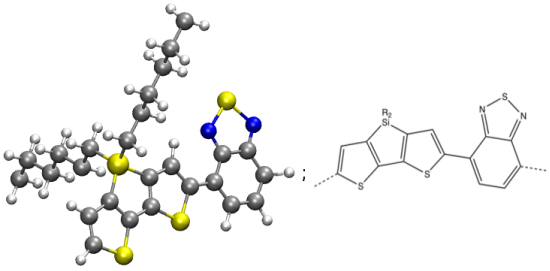

Figure 1.7: Co-polymer of dithienosilole and benzothiadiazole (visual and schematic repr.)

1.3.2 PSBTBT-6

BHJ big interfacial area can be achieved through the phase separation between the two components in bulk. The long hydrocarbon chains bonded to the silicon atom help, hosting fullerene derivative clusters of molecules. Those regions are somehow interconnected to assure conductivity among electrodes, the backbone of the copolymer needs to do so also. In order to simulate this donor-acceptor interface it was thought necessary to start from a not too small unit cell. In y and z direction to avoid interactions that will increase difficulty reaching equilibrium. In the x direction, however, the cell is adjusted to fit perfectly to the oligomer chosen. Our selection for all the calculations is a tetramer Figure 1.6, such as **-ad-ad-ad-ad-** according to the naming given in Figure 1.6. Its length is enough to make possible to picture twists and other conformational changes after the dynamics.

It is important to mention that the initial backbone structure of the copolymer is very much in a plane assuring a π-orbitals delocalization over the whole tetramer.

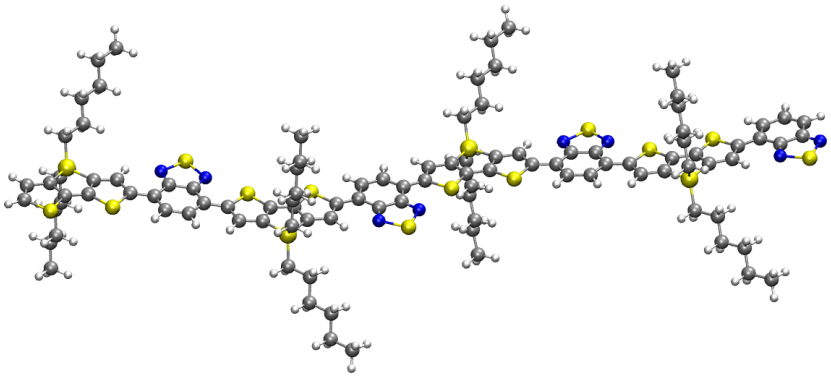

Figure 1.8: poly(4,4-dihexyldithieno(3,2-b:2',3'-d)silole-2,6-diyl-alt-(2,1,3-benzo-thiadiazole) -4,7-diyl): Tetramer of Figure 1.7 used during the calculations.

1.3.3 PCBM

As it has been mention, PCBM (c.f., Figure 1.9) is one of the acceptor molecules preferred in OPV, as not substantial performance improvements have been observed so far by replacing PCBM with similar compounds or other n-type materials. Due to it proven functionality it was selected as a comparison for the posterior functionalization.

PCBM, unlike C_{60}, is soluble in common organic solvents such as toluene, monochlorobenzene, ortho-dichlorobenzene and dichloromethane which make it very appropriate for the fast processing techniques used in OPVs production. In addition, it preserves important electronic and optical properties of the parent fullerenes while providing a significant increase in solubility and processability.

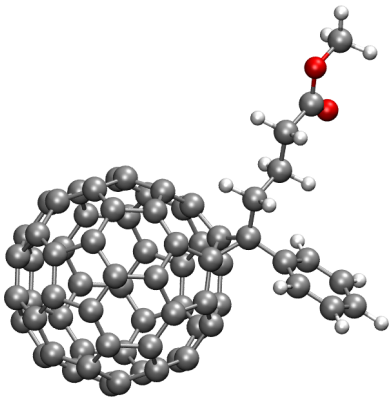

Figure 1.9: [6,6]-phenyl C61-butyric acid methyl ester

1.3.4 PCBPP

In inorganic crystals, the strong dielectric constant implies an effective shielding of coulomb forces, this is not the case in organic BHJ blends due to their low dielectric constant. It implies that when an optical transition is to take place, in order for an electron to escape from its coulombically bound sibling, it had to overcome a coulomb capture radius which is about 20 nm. It was hypothesized within the FOM Focus Group[3] that substituting the PCBM molecule with molecules possessing a high dipole will help to increase the stabilization of the generated charges.

A molecule as p-nitro-N,N-dimethylaniline has a dipole μ $0.104 mm^{-1}$ [26], was thought ideal to be used as a substituent and molecule in Figure 1.10 was therefore chosen for the subsequent calculations.

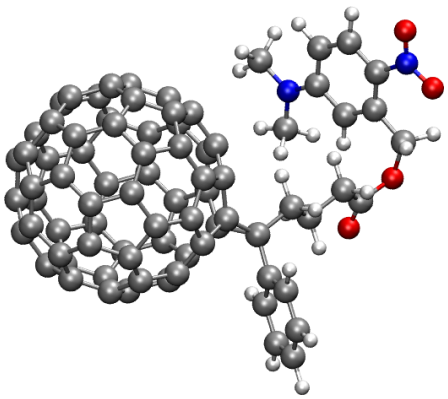

Figure 1.10: [6,6]-phenyl-C61-butyric acid (2-N,N-dimethylaniline-5-nitro)benzyl ester

1.4 Modeling Techniques

1.4.1 Density Functional Theory

Electronic structure calculations attempt to determine the total energy of a system of nuclei and their electrons. Knowledge of the total energy of a structure is cumbersome but important in a theoretical investigation. The structures considered in this work correspond to complex systems with a large number of degrees of freedom. It is therefore necessary to make a number of simplifications on the ideal approach.

[3] http://www.groningensolar.nl

The motion of electrons and nuclei are described by the many-body Schrödinger equation. Within the Born-Oppenheimer approximation one separates the motion of the electrons from the motion of the nuclei so that for given nuclear positions in a first step it is only needed to solve the many-electron Schrödinger equation. With this solution one can in a second step calculate the forces on the nuclei, optimize the nuclear positions with respect to the total energy and hence derive the equilibrium geometry.

The many-electron Schrodinger equation is usually solved using either wavefunction based methods such as the Hartree-Fock formalism or electron density based schemes such as density functional theory (DFT). The latter circumvents the computationally expensive aspects of theory by treating the *electron density* with only *three degrees of freedom* as the fundamental variable instead of the full wavefunction with $3 \cdot N_{electrons}$ degrees of freedom.

1.4.2 Density Functional Tight Binding

As stated before, predicting chemical properties is one of the main tasks in theoretical chemistry. There are a great number of methods available to do so, each one being most adequate for a particular scenario.

In principle, all knowledge about a system can be obtained from the quantum mechanical wave function. This is obtained (non-relativistically) by solving the Schrödinger equation of the complete many-electron system. However, in practice solving such an N-body problem proves to be impossible. The high accurate post Hartree-Fock methods would be computationally prohibitive for the systems treated here. Also to have an accurate description of the systems treated, a method which considers quantum effects would be desired since they contains large π-conjugated subunits. In order to increase the computational efficiency while maintaining the theoretical accuracy at the same time, the density functional based tight binding (DFTB) method [27, 28, 18] is employed. DFTB is a method developed in the mid-1990s. It is derived from density functional theory (DFT) by approximation and parametrization of the interaction integrals [27] and [29]. The performance for geometries is very well and comparable to DFT results in many calculations (i.e., Ohta et al.[30]).

Self-consistent charge density functional tight-binding (SCC-DFTB) [29, 31] (hereafter abbreviated with DFTB, as it was the only method used) constitutes an alternative to the traditional semi-empirical (SE) methods in Quantum

Chemistry, the most well know being AM1 and PM3 schemes, which are derived from Hartree-Fock theory. Formally, it has some similarity with extended Hückel theory. However, DFTB is not a semi-empirical method in a strict sense, since its parametrization procedure is completely based on DFT calculations, no fit to empirical data has to be performed. In contrast to most SE methods DFTB is a non-orthogonal method, that is, it is based on a non-orthogonal basis set, a key factor for transferability [32]. Transferability denotes the ability of a parametrized method to perform sufficiently well also for chemical environments not included in the parametrization procedure. Roughly speaking, DFTB gives results closer to the DFT ones whenever there is a difference with respect to *Ab Initio* methods[33, 29]. Of course, problems of the current DFT functionals are also inherited, like the overpolarization in conjugated systems which leads for example, to an underestimation of the bond alternation and the related problems in the description of ionic and charge transfer excited states, or the neglect of dispersion forces. However Prof. Niehaus from the University of Regensburg has successfully performed several calculations on excited states. At this very moment, the code is still not opensource. Therefore, the initial aim of studying charge transfer states, from the generated initial geometries, has been postponed to the future development of the Tight Binding (TB) approach into the used DFTB+ software package[34, 35] it was mentioned, the TB model can be rigorously derived from density functional theory [27] and this will be briefly discussed in the next paragraphs.

Summarizing the tight-binding approximation provides a methodology for atomistic modeling of these systems as it allows to investigate the electronic behavior at low computational cost while retaining the accuracy.

1.4.2.1 Derivation of the Tight Binding model

The easiest way to understand DFTB is to start from the Fock equation with the framework of the Hartree-Fock-Roothaan approximation. First of all, it is assumed that there exists a minimal set of short-range basis functions. These functions can be orthogonal or non-orthogonal to each other. The explicit form of the functions is not needed because the matrix elements will not be evaluated but approximated as analytical functions of atomic coordinates.

The total energy E_{tot} of the electron system is represented as a sum of the electronic energy and pair terms, but instead of the Coulomb equations, an ana-

lytical short-ranged function f of atom positions is introduced. Self-consistency is neglected completely, or approximated in the expression for the electronic energy (which actually means that the repulsion of two electrons only is accounted when they are localized near one and the same atom). The zeroth order approach is equivalent to a common standard non-self-consistent (TB) scheme, while at second order a transparent, parameter-free, and readily calculable expression for generalized Hamiltonian matrix elements can be derived. These are modified by a self-consistent redistribution of Mulliken charges (SCC). At large distances this accounts for long-range electrostatic forces between two point charges and approximately includes self-interaction contributions of a given atom if the charges are located at one and the same atom. Due to the SCC extension, DFTB can be successfully applied to problems, where deficiencies within the non-SCC standard TB approach become obvious.[4]

In case a further insight is needed please go to the appendix A, where a detailed derivation of the tight-binding model is presented.

1.4.2.2 Self-consistent charge DFTB

SCC-DFTB is derived from DFT by choosing a reference density ρ_0 as a superposition of neutral atomic densities ρ_0^α, $\rho_0 = \sum_\alpha \rho_0^\alpha$ and expanding the DFT exchange-correlation up to the second order as shown in Eq. (1.2):

$$\begin{aligned} E &= \sum_{\alpha}^{occ} \left\langle \Psi_i | \hat{H}_0 | \Psi_i \right\rangle - \frac{1}{2} \iint' \left(\frac{\rho_0^\alpha \rho_0^{,}}{|\vec{r} - \vec{r}'|} \right) + E_{xc}\left[\rho_0\right] - \\ &- \int V_{xc}\left[\rho_0\right] \rho_0 + E_{ii} + \\ &+ \frac{1}{2} \iint' \left(\frac{1}{|\vec{r} - \vec{r}'|} + \left. \frac{\delta^2 E_{xc}}{\delta\rho\delta\rho'} \right|_{\rho_0} \right) \delta n \delta n' \end{aligned} \tag{1.2}$$

In this equation it is possible to identify a sum over the Kohn-Sham eigenstates Ψ_i, an exchange correlation (XC) part, the correction for double counting the Hartree energy and $\hat{H}_0$ as the Hamiltonian operator resulting from an input density n_0.

[4] http://www.dftb.org/about_dftb/

The traditional non-self-consistent-charge TB (Zeroth-order non-self-consistent charge) approach is to neglect the last term in the final expression in Eq. (1.2). As usual, a frozen-core approximation is applied to reduce the computational efforts by only considering the valence orbitals. The Kohn-Sham equations are solved non-self-consistently and the second-order correction is neglected. The contributions in Eq. (1.2) which depend on the input density n_0 only and the core-core repulsion are taken to be the sum of one- and two-body potentials [27]. The latter, denoted by E_{rep}, are strictly pairwise, repulsive and short ranged. The total energy then reads:

$$E_0^{TB} = \sum_i^{occ} \left\langle \Psi_i | \hat{H}_0 | \Psi_i \right\rangle + E_{rep} \tag{1.3}$$

In order to solve the KS equations, the single-particle wavefunctions ψ_i within a LCAO are expanded into a suitable set of localized AO ψ_v,

$$\psi_i(r) = \sum_v c_{vi} \varphi_v(r - R_\alpha) \tag{1.4}$$

By applying the variational principle to the zeroth-order energy functional 1.3, it is possible to get the non-self consistent field KS equations, which, finally, within the pseudoatomic basis, transform to a set of algebraic equations:

$$\sum_v c_{vi}(H_{\mu\nu} -_i S_{\mu\upsilon}) = 0; \ \forall \mu, i \tag{1.5}$$

By solving the general eigenvalue problem, Eq. (1.5); the first term in Eq. (1.3) becomes a simple summation over all occupied KS orbitals with energy ϵ_i, while E_{rep} can easily be determined as a function of distance by taking the difference of the SCF-LDA cohesive and the corresponding TB band-structure energy for a suitable reference system.

1.4.3 Molecular dynamics simulation

Quantum molecular dynamics is quite different from classical molecular dynamics, which is primarily concerned with the classical motion of atoms interacting with a given potential. The interesting chemistry and physics of many molecules take place at the atomic and subatomic level. But Newton's laws of classical me-

chanics no longer apply here. Physicists developed quantum mechanics early in the 20th century to appropriately describe the physics and chemistry of matter at the microscopic level. Quantum molecular dynamics focuses on all the interactions between atoms and electrons and does not involve fitting interactions to experimental data. First-principles, or *ab initio*, molecular dynamics models use only the laws of quantum mechanics, the fundamental physics equations that describe electrons. This is unfeasible for the size of the systems under study.

Molecular-dynamics simulation has been attracting a lot of interest due to its powerful capabilities to give relevant insight for the behavior of systems in time as a function of temperature, or in the investigation of kinetics in various processes, as well as in locating the ground state of complex systems with many degrees of freedom. However, the application of the method to real systems is limited by our knowledge of the interaction potentials or forces among the atoms. The simulation of interatomic forces for molecular-dynamics in real systems therefore provides an important goal and a significant challenge to theory. Such is the case, for example, for the molecular-dynamics simulation of the materials used in organic photovoltaics. The problem here is that the methods of coarsening the description from atomistic to nanoscale are not as obvious as it is in going from electrons to atoms.

DFTB employ a potential energy function (referred to as a force field) that calculates the overall potential energy of the system based on the summation of individual atom-atom pair interactions. The force field equation takes into account the contributions due to bonded interactions (bond stretching, bending, and torsion) as well as non-bonded interactions (van der Waals and electrostatic). These energy contributions are determined by a set of empirical parameters that are used by the force field to calculate the energy contribution for each type of interaction for the atom types that are defined in the molecular system under consideration. To accurately simulate molecular behavior using an empirical force field, parameters of the force field must be balanced and tuned together to appropriately represent the behavior of the given molecular system being addressed. As a consequence of this, a force field designed for one type of application cannot be confidently applied to other applications without separate validation; this issue is known as force field transferability, similar to the statement in section 1.3.2.

The main ingredient of a simulation is to create a realistic physical model. For a molecular dynamics simulation, this means choosing a potential or force field, function $V(r_1, ...r_N)$ of the positions of the nuclei, representing the potential

energy of the system when the atoms are arranged in a specific configuration.

The forces are then derived as the gradient of the potential with respect to atomic movements as it is shown in eq. 1.6:

$$F_j = -\nabla_{r_i} V(r_1, ...r_N) = -\nabla_{r_i} \sum_i \sum_{j>i} \phi(r_i - r_j) \tag{1.6}$$

The simplest choice for V is written as a sum of pair interactions $\phi(r_i - r_j)$. The second summation index $j > i$, tells us to consider each pair just once.

The choice of force field depends in large part on the system to be studied and its properties to be investigated. Beyond refined description of the relevant atomic vibrations, the conformations of macromolecules depend more on the twists, the repulsion, van der Waals attractions and electrostatic interactions.

In the present research, a quantum chemical MD method based on the density functional tight-binding (DFTB) method [29] combined with a finite electronic temperature approach is used [36]. The DFTB method allows to carry out electronic structure calculations that are at least two orders of magnitude faster than the first-principles density functional theory (DFT), and provide remarkably similar energies and structures [30].

Throughout this work, two of these methods of geometry optimization were used i.e., the conjugate gradient relaxation and molecular dynamics methods. Both of them can be used within the SCC-DFTB code[18, 29].

Conjugated gradient This algorithm is used for finding its local minimum under the assumption that the gradient, for a function of n variables, can be computed. It is the oldest and best known non stationary method for solving positive definite systems effectively.

Verlet algorithm Molecular dynamics are propagated by using Verlet algorithm, which makes it possible to take time steps in the order of those that are standard in molecular dynamics simulations with an empirical potential energy function.

1.5 Aim of the thesis

In the first sections of this thesis the general concepts necessary to understand OPV system were introduced. Already a significant research effort is put into developing these materials as it can be inferred from the references. There are two strategies to improve the performance beyond that of the initial P3HT:PCBM solar cells. Firstly, testing other small band gap polymers that can be used to enhance the light absorption of the solar cell. Lastly, verify if other acceptors with more suitable HOMO-LUMO levels can be employed to increase the charge transfer. In order for this research effort to be successful it is crucial that materials are understood from both sides, theoretical and experimental.

It is possible to say that fullerenes have always been the acceptor of choice when making polymer solar cells. So far efficiencies have remained being moderate. We will focus on theoretically model equilibrated structures of mixtures of fullerene derivatives and a typically used polymer, and to evaluate the effects of adding functional groups to the PCBM.

Starting with a monodimensional arrangement in order to gain understanding in the pros and cons of applying this methodology and by looking at properties such as, the shifts on the density of states plots, or the charge distribution upon complex formation, it will be possible to evaluate differences on the behavior of these alike mixtures.

MD simulation on copolymer-fullerene derivatives had been performed trying to evaluate some interesting properties, by first hypothesizing different systems and then analyzing several snapshots of each MD run. This is done in order to sample a broad spectra of possible configurations that are at the end the inputs needed in subsequent higher level calculations.

To conclude, the aim was to gain an understanding of DTFB theory and also to apply this methodology to the complex processes of predicting interfaces arrangements; to model these structures and determine ground state properties in general and more particularly the consequences of adding a dipole. All of this should lead to a better understanding of bulk heterojunction properties in the future.

Limitations

These calculations are demanding and the time-frame available limited, therefore all models have been simplified.

The relation between the morphology and associated device properties in conjugated polymer/fullerene bulk-heterojunction for solar cells have been investigated by e.g. Hoppe et al. in 2004 [37]. The existence of collaborative effects within the 3D domains of the percolated solid state blends have been demonstrated; but in these simulations all models have been simplified to 1D (although 2D were already equilibrated but they were not taken into further analysis).

It is assumed that it is possible to keep the cells at constant temperatures at all time. In reality, absorption, especially with a large influx of photons, will produce excess heating of the solar panels.

Chapter 2

Computational framework

Chapter two is dedicated to the description of both the computational procedures and the systems used.

Science is a wonderful thing
if one does not have to earn one's living at it.
Albert Einstein

2.1 Periodic boundary conditions

To describe these systems in a solid state basis it is necessary to perform the MD using periodic boundary conditions (PBC). This is the classical way to minimize edge effects in a finite system. The atoms of the simulated system are put into a periodically space-filling box containing all the representative atoms (called unit cell), which is treated as if it is surrounded by other unit cells, reassuring an apparent but effective periodicity. In the first set of calculations the system is in a P_1 triclinic lattice with a large inter-polymeric separation to avoid interaction between the fullerene derivatives in two different layers (c.f. Figure 2.1) the polymer itself is arranged such it follows the $\vec{a}$ vector of the cell. In a subsequent step a 2D structure was proposed although no properties were evaluated further for it. In this configuration, interactions are allowed in $\vec{a}$ and $\vec{c}$ directions (not in $\vec{b}$).

The numerical results (density of states, band gaps, charge distribution) were obtained for the primitive unit cell in PBC, containing 424 and 464 atoms, for the PCBM and PCBPP systems respectively. The Brillouin zone of these structures was sampled by 4 k-points. The energy convergence criteria should be better than $1.0e^{-6}V/atom$ during the self-consistency iterations. A maximum force on atom sites of $1.0e^{-4}eV/\AA$ was criterion for the convergence of the initial conjugated gradient structural optimizations (initial relaxation).

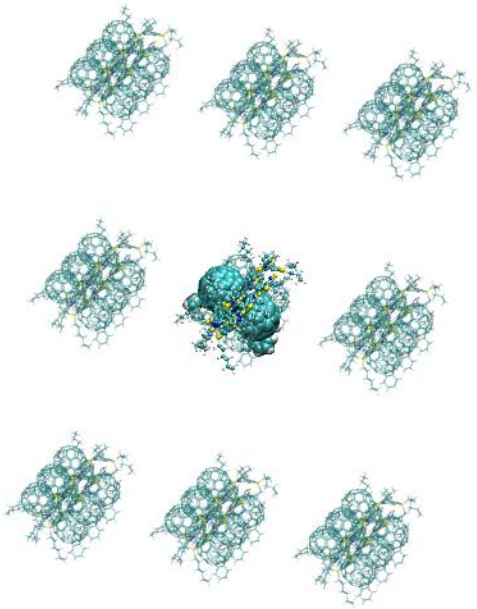

Figure 2.1: Real periodicity of the systems in only one direction

2.2 Systems

In order to cover various possible initial configurations of polymer and the fullerene derivatives, 24 initial spatial conformations were hypothesized in a pretty much random way. In a subsequent selection only three of them were selected according to the proper evolution and finalization of the MD, the total energy criteria - the lower the better - (it is actually necessary to look at the Mermin energy as a small electronic temperature is used) and finally fullerene-fullerene distance. The latter, allows to classify them into short, long and medium fullerene-fullerene distance; ranging from ~7Å to ~20Å. In Figure 2.2 those selected ones are presented; three for the copolymer-PCBM and three for the copolymer-PCBPP systems. They are numbered as four, five and six, the letter refer to the p-nitro-dimethyl-aniline substituted PCBM if it is (**A**), or pristine PCBM if it is (**B**). The initial structures for each of the couples were the same, the only difference is the added p-nitro-N,N-dimethylaniline on A at the end chain containing the ester (after geometry

relaxation of B).

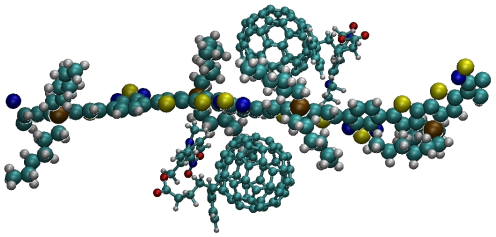

(a) A4 (PCBPP/PSBTBT-6 mix)

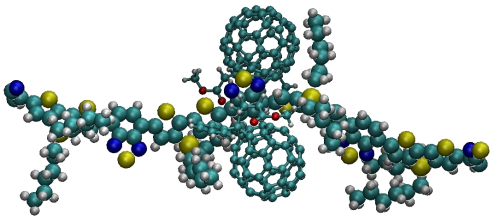

(b) B4 (PCBM/PSBTBT-6 mix)

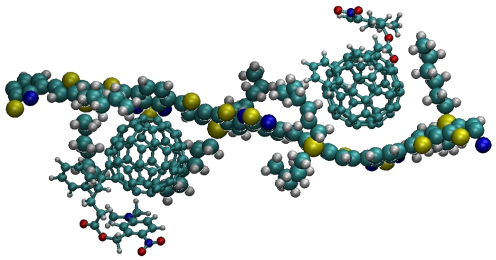

(c) A5 (PCBPP/PSBTBT-6 mix)

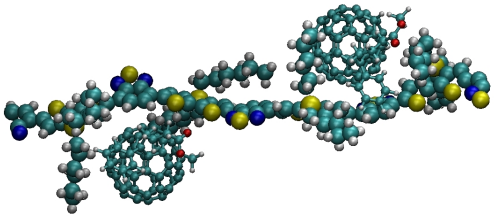

(d) B5 (PCBM/PSBTBT-6 mix)

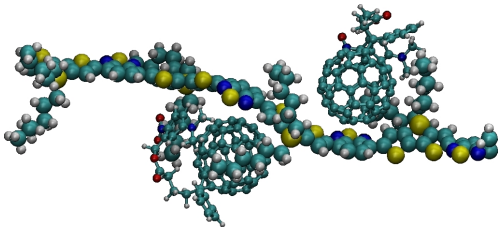

(e) A6 (PCBPP/PSBTBT-6 mix)

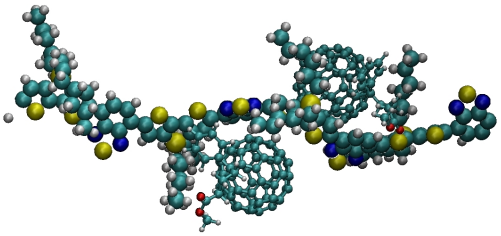

(f) B6 (PCBM/PSBTBT-6 mix)

Figure 2.2: Systems conformation after 11.5ps of MD

2.3 Practical usage of DFTB+

All QM/MD simulations employed the self-consistent-charge density-functional tight-binding method (SCC-DFTB) [18, 29]. DFTB is an approximate density functional theory method based on the tight binding approach and utilizes an optimized minimal LCAO Slater-type all-valence basis set in combination with a two-center approximation for the Hamiltonian matrix elements.

The DFTB wave function, energy and gradient were computed at each MD step. A low electronic temperature (T_e) [38] of $100K$ was enforced on the DFTB wave function: On the one hand, orbital occupations can be approximate to a Fermi-Dirac distribution that varied almost discretely (0 or 2) near the Fermi level, on the other hand, it assures a faster SCC convergence. The Newtonian equations of the motion of nuclei were integrated using the popular Velocity-Verlet algorithm [39], which is one of the most popular MD integration

schemes nowadays. In this algorithm both the nuclear coordinates and velocities are updated at each iteration of the integration, using coordinates/velocities of the previous iteration. The NVT ensemble was maintained by applying the Nose-Hoover chain thermostat [40, 41, 42]. The nuclear temperature was set to $300K$ throughout all simulations and the analyzed snapshots belong to the region of equilibrium (see Figure 3.2 in the next chapter).

2.4 DFT calculations

The orbitals and the charge distribution were also calculated using a pure DFT approach. The structures of the systems (c.f. Figure 2.2) were completed with the missing hydrogens in order to perform a cluster calculation and then imported into ORCA and optimized using Density Functional Theory (B3LYP as a functional) with a 6-31G(d) basis set to determine both the molecular orbitals and the charge differences upon complex formation. This accomplished the aim of finding good agreement with the DFTB results as it was expected (c.f., appendix B).

Chapter 3

Results and discussion

The main goal of the research was to simulate blends using the DFTB technique, in order to elucidate the influence of PCBM functionalization on the morphology of the bulk heterojunction.

The interdigitated structure of solar cells is inherently linked to the 3D geometry and obviously a 1D geometry is just a first stab to modell the complex BHJ interface using DFTB.

Dat heeft u weer. Feiten die er niet om liegen.
Bewijzen om u tegen te zeggen.
U mag niet omvallen. Gelooft u mij.
Het is nog veel te vroeg.
Anneke Claus

3.1 Structure evolution

In Figure 3.1 the conformation changes along the MD trajectory are shown. These type of systems have may degrees of freedom and it is very costly to do a systematic geometry evolution, the MD algorithm allows the study of the dynamics of the molecules (sampling many possible conformations along the trajectory). Figure 3.1a shows the very initial step of the simulation. The structure comes from a geometry relaxation that adjust slightly bond lengths and angles but the displacement of the constituents is not observed. Figure 3.1b is a snapshot half

way through the MD trajectory. It is easy to see that significant changes have occurred. However the simulation is still at a very early stage (not equilibrated) and changes might be very large. The copolymer bends and twists even made the fullerenes to separate. However, in Figure 3.1c the fullerenes look again closer, and the initially drastic twists have been smoothed. This is typical for the equilibrium region.

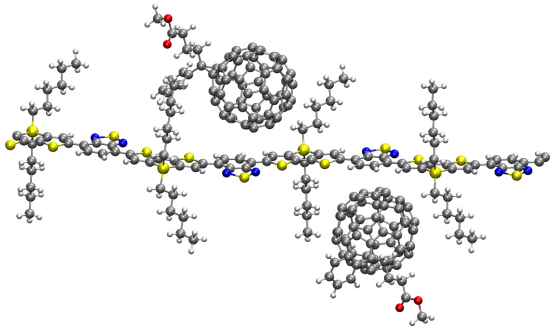

(a) Initial structure for B6 after preoptimization (almost flat)

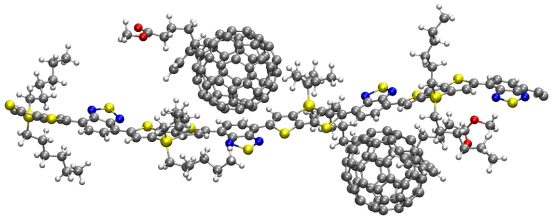

(b) Intermediate structure for B6 (many twists and some movements of the fullerene derivatives)

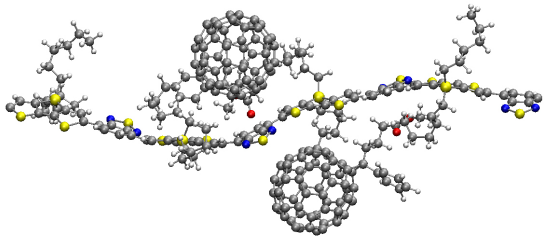

(c) Final structure for B6 (the twists remain although they seem more armonic, the position of the fullerene derivatives are closer to each other)

Figure 3.1: Conformational changes along the simulation for system B6.

System **A**	Total Mermin free energy [H]	System **B**	Total Mermin free energy [H]
1	-602.8097530829	1	crash
2	-602.5863145821	2	-546.8126615036
3	-602.8063416443	3	-546.8012154236
4*	-602.5263474032	4*	-546.8079981261
5*	-602.7624708990	5*	-546.7531227472
6*	-602.7911040276	6*	-546.773696981
7	-602.8079331623	7	-546.7875424393
8	crash	8	-546.8451638993
9	-602.8210741308	9	-546.8150653631
10	-602.7601431519	10	crash
11	-602.7930237806	11	crash
12	crash	12	-546.8269758546

Table 3.1: Energy and temperature at the final MD step for each one of the systems (Those marked with * are the selected ones)

This is obviously a very complex process and therefore some of the 24 initial structures had problems along the dynamics and either crash or took too long to take them into consideration. From those that finish we check the final energy (see Table 3.1) and the relative position of the fullerene derivatives. The six selected were the starting point, as mentioned, for the subsequent statistical analysis. The initial geometries are therefore a result of an educated guess of 24 systems where the fullerene derivatives were place in many possible positions.

3.2 Morphology and band gap

One-dimensional simulations can be a first approach to solar cells behavior, especially for semiconductor materials that are not well characterized yet. To increment the validity of the study a statistical analysis was performed in order to analyze the 300 snapshots generated for the systems. These snapshots were gathered from an equilibrated part of the simulation (from 6ps to 11ps, zone between the yellow lines in Figure 3.2, and assuring little interrelationship among them). Then some properties were evaluated for those in order to try to establish a solid ground where to interpret the results of -higher dimensionality- future calculations.

	Total MD Energy [H]	MD Temperature [K]
A4	-601.48825	302.1369
B4	-545.45710	285.4248
A5	-601.50343	289.0642
B5	-545.48932	294.7509
A6	-601.50898	289.0642
B6	-545.49230	300.1114

Table 3.2: Energy and temperature for the solid state calculations for each one of the systems

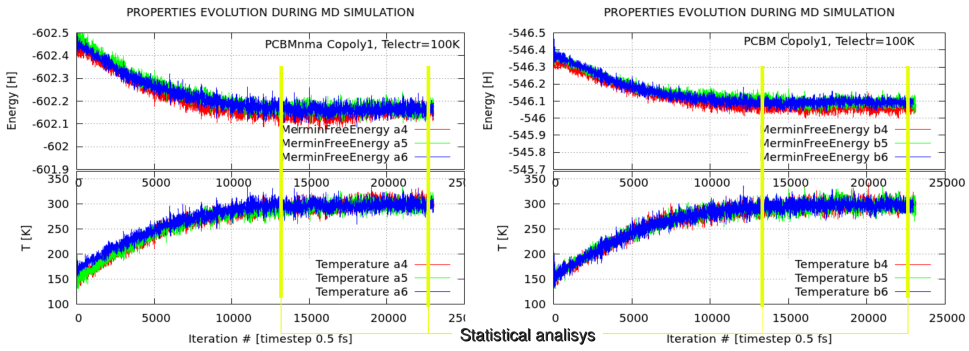

Figure 3.2: Energy and Temperature evolution for all systems.

At this point it is important to point out that the variation in the final energies behavior is very subtle (see Table 3.2). As it is possible to see in the upper part of Figure 3.2 even for three systems (4, 5, and 6) that are significantly dissimilar, the evolution in the energy overlaps pretty well. This can be interpreted like the systems energetic stability is not totally driven by the position but for the constituents.

It is true that the mobility of a monodimensional system is larger than a tridimensional one but as far as we are modeling at 300K and the cells will heat up under sun radiation, some movement is expected. It also is possible to suppose than a 3D packing will allow smaller movements on the structures and therefore the band gap fluctuation will diminish. This partial mobility, in the other hand, may be helpful at a later stage to stabilize the charge separation and charge migration processes.

As far as our intention is to understand the morphology behavior, in Table 3.3 are summarized a few important morphological characteristics averaging all the 300 snapshots.

The distances in Table 3.3 are the PCBM-PCBM (or PCBPP-PCBPP)

	full1-full2 c.o.m dist	minimal dist ful1-ful2	dist full1 to polymer ⊥	dist full2 to polymer ⊥
A4	13.18 ±0.13Å	6.14 ±0.16Å	3.10±0.11 Å	3.11±0.12 Å
B4	13.16±0.25 Å	6.27±0.26 Å	3.10±0.18Å	3.16±0.15 Å
A5	22.20±0.61 Å	15.30±0.62 Å	3.13±0.11Å	3.18±0.15Å
B5	25.01±0.45Å	17.50±0.44 Å	3.16±0.12 Å	3.11±0.13 Å
A6	15.82±0.73 Å	8.77 ±0.80 Å	3.14±0.13Å	3.17±0.10Å
B6	15.46±0.87 Å	8.45±0.82Å	3.14±0.14 Å	3.15±0.14 Å

Table 3.3: Morphological distances of the components of the systems, averages of all snapshots

	placement full at first snapshot	placement full at last snapshot
A4	benzothiadiazole	dithienosilole /benzothiadiazole
B4	benzothiadiazole +	benzothiadiazole -
A5	dithienosilole / benzothiadiazole	dithienosilole / benzothiadiazole
B5	benzothiadiazole	benzothiadiazole
A6	dithienosilole / benzothiadiazole	dithienosilole -
B6	dithienosilole / benzothiadiazole	dithienosilole -

Table 3.4: Placement of the (nearest) fullerene derivative with respect to the copolymer subunits at the beginning and at the end of the MD

center of mass distances; the minimal distance between two atoms, one of buckyball1 and the other of buckyball2; the last two columns represent the perpendicular distances between each one of those and the polymer backbone. One possible result to extract from here is that when the fullerene derivatives are farther away it is more likely that the distances varies whether looking at systems B or at system A. Therefore, collaborative effects of fullerene clustering became expected when looking at Table 3.3 standard deviation value. These give much relevancy to the next step of higher dimensionality calculations.

In Table 3.4 it is possible to observe the variation of the preferred position of the fullerene derivatives in a time dependent situation. The symbols + and - are to emphasize the "overlap" the buckyball with the subunits of the copolymer: the maximum situation will have not sign, then + implies a quite big overlap and - when it is subtle.

It is paramount to mention that along the simulations the fullerene derivative moves slightly from the initial position, while the polymer moves much more and it is obvious that the donor molecules tent to wrap around the fullerenes in a very proactive way.

In conclusion, the buckyballs prefers to sit above the interconnection of

two consecutive donor acceptor fragments.

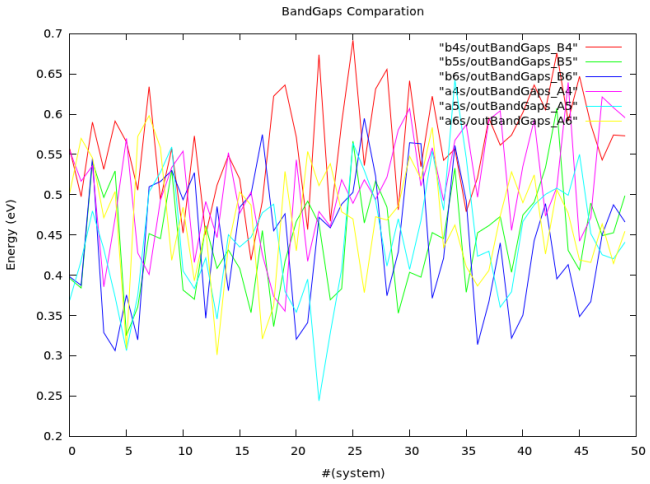

Figure 3.3: Band gap energy vs. snapshot structure

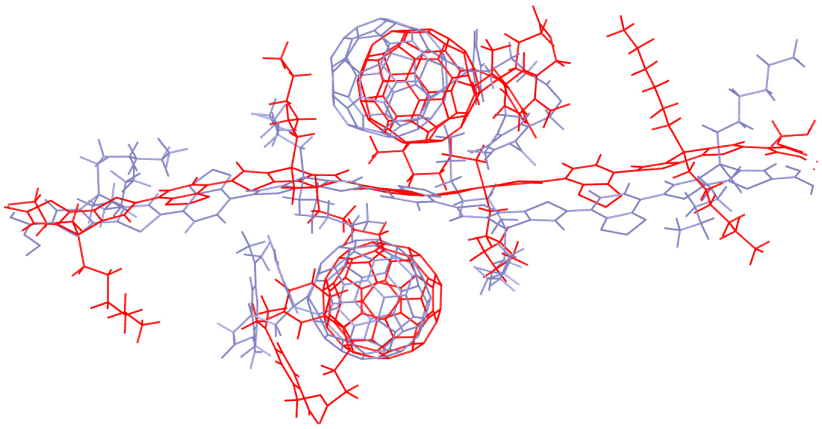

(a) Structural differences for A4

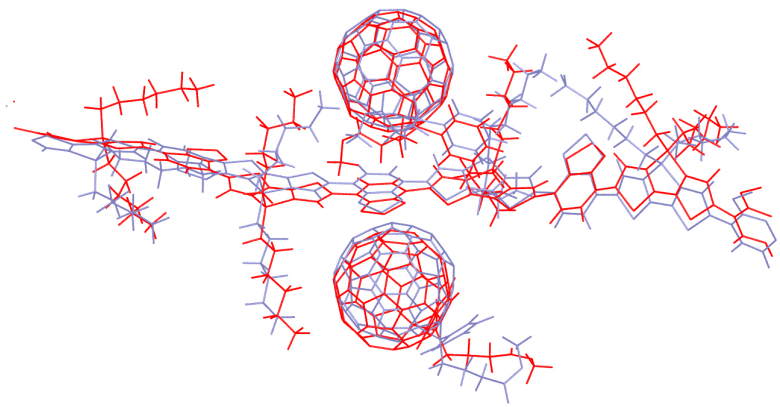

(b) Structural differences for B4

Figure 3.4: Visual representation of the differences amongst structures with the larger (system25: red) and the smaller (system16: blue) band gaps for two of the systems studied.

Evidently, material properties of the donor and acceptor also have a direct impact on the performance of OPV devices as they determine e.g., light absorption, mobility of free charges, the value of the open circuit voltage, etc. As it is shown in Figure 3.3 the band gap depends on the selected snapshot and therefore on the spatial arrangement of the molecules within the complex as is shown in Figure 3.4. Another important result that can be extracted from here is that apparently the planarity of the polymeric backbone, and hence the π-conjugation along the polymer, is somehow interconnected with the systems band gap. The less twists the larger the band gap (c.f. Figure 3.3 and Figure 3.4). This will probably affect broadening the energy bands. In addition to this, it must be acknowledged that the variations of the band gap are in the same order of magnitude.

The changes are quite important and this emphasizes how relevant it is to obtain significant initial structures, for the subsequent *pure*-quantum calculations.

3.3 Charge redistribution

The charge redistribution, or polarization effects, induced by the presence of both types of systems can be visualized in the pictures. The electrostatic force binds electrons and nuclei together to form atoms and the same force holds atoms and molecules together in bulk material. However, the behavior match the typical interaction effects among molecules in the bulk although the interaction is very small if it is compared with the interaction in a typical crystalline solid.

It is possible to see how there is a region with negative (blue) net charge (after the complex is formed and subtracting the charge of isolated atoms), placed in the fullerene, if a more positive (red) is localized in the polymer area. It is worth to notice that the isosurfaces used are very small, and therefore these changes are very subtle however non-negligible.

As it has been said, the behavior is similar to typical interaction effects between different atoms or molecules; in both figures there is a slight interaction, qualitatively presented in Figure 3.5, however there is a particularity easy to observe. System B4 charge differences are somehow focused in the area near the fullerenes and for system A4 the charge differences are obvious along the whole polymer backbone.

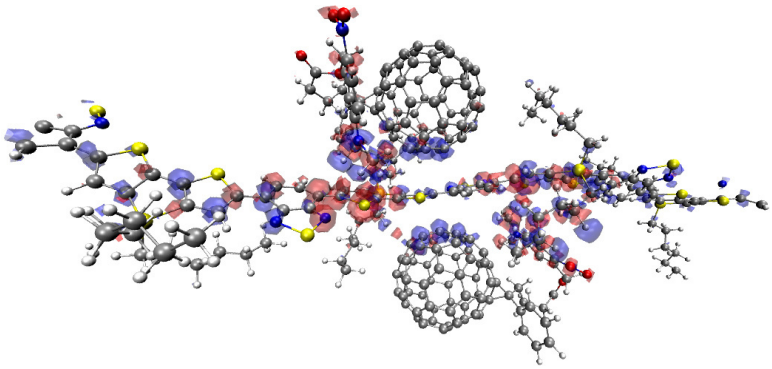

(a) A4 charge difference (isosurface 0.0002)

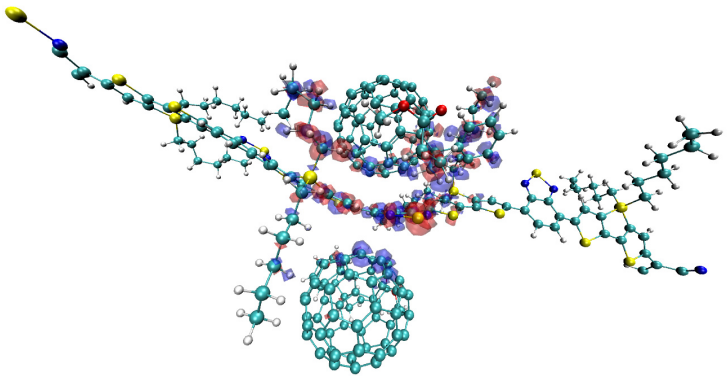

(b) B4 charge difference (isosurface 0.0002)

Figure 3.5: Visual representation of charge redistribution upon complex formation

3.4 Density of states

The pictures grouped in Figure 3.6 are plots of the total density of states (DOS) and of partial density of states (PDOS) for all the systems we are dealing with. The major point of interest here is that partial occupied densities of states (DOS) of each chemical species within the compound can be compared with the species isolated.

The presented plots of the DOS of the systems investigated have some interesting particularities that are very much worth to mention. Although all the plots will be commented and interconnected in a general way, systems A4 (c.f. Figure 3.6a) and B4 (c.f. Figure 3.6b) will be analyzed in more depth.

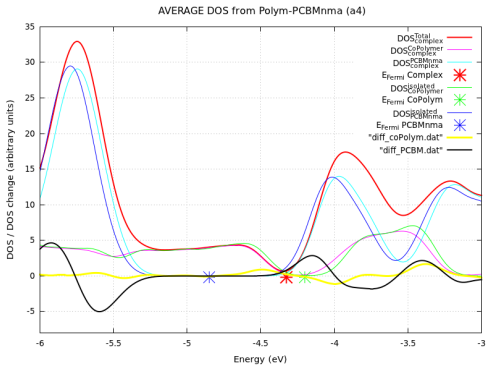

(a) A4 average DOS, comparative diagram

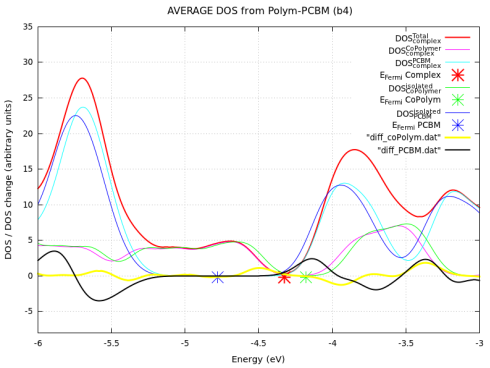

(b) B4 average DOS, comparative diagram

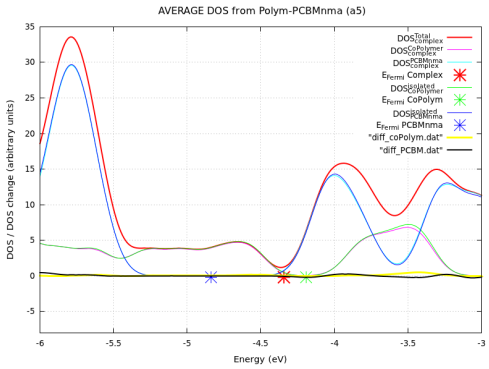

(c) A5 average DOS, comparative diagram

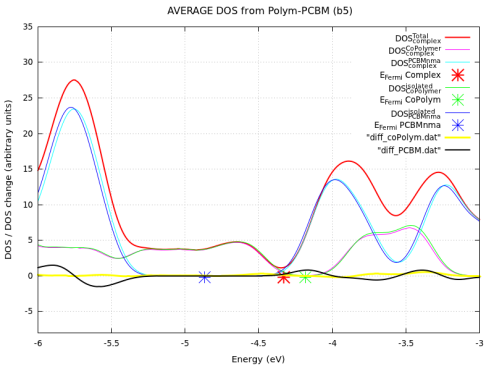

(d) B5 average DOS, comparative diagram

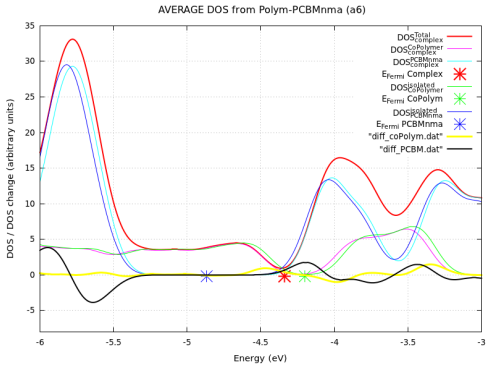

(e) A6 average DOS, comparative diagram

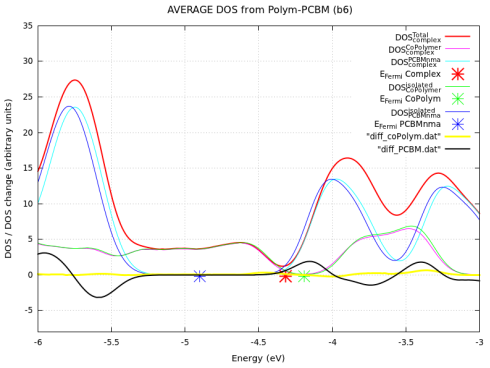

(f) B6 Average DOS, comparative diagram

Figure 3.6: Statistical study of DOS and PDOS of the different systems. The color code used is the following: the red line is the total dos of the complex, this is subdivided in partial contributions: purple and light blue, that can be compared with the calculated DOS for the individual components: green the copolymer and dark blur the fullerene. In black the fullerene differences, and in yellow the polymer differences.

It is interesting to point out the shifts of the density of states of the isolated molecules and the same molecule(s) but as PDOS within the complex do not overlap. Looking at the variations it can be concluded that in mostly every case the density of states of the fullerene derivative is displaced to less negative

values while the polymer on the other hand shifts the opposite direction. A plausible way to interpret this is that the buckyball part is less prone to receive more electrons once the complex is all together. It may mean that it already received some electronic density from the copolymer. The copolymer behaves like it is not willing to give electrons anymore after the complex is formed. This is probably caused by the fact that it already gave some electron density to the fullerene derivative. Of course this is just one of the possible interpretations for these schemes but is however plausible, according to the Mulliken charges data gather at the end of the calculations.

Focusing in the systems where the fullerenes are closer (A4 and B4), it is possible to mention some more gripping peculiarities. Interesting is to mention how these close shell systems present similar values for the Fermi energy, so happen for the band gap, although the conformation is rather different. The band gaps for each independent part parts is smaller that the values reported in the literature for similar systems HOMO–LUMO gap's. Although it is known that DFT methods, and hence DFTB, generally underestimate energy band gaps they can still provide qualitative trends [43]. It is possible to observe similar shifts on the PDOS with the only particularity of an increase of on the intensity of the peak for the HOMO of the fullerene for the B4 with respect to A4 which is probably correlated with a more stable HOMO for the complex. More important is to notice that the shifts in 4 are bigger than in 6 and those bigger than in 5. It could mean that systems in which the fullerene-fullerene distance is smaller the electronic interaction between the copolymer and the fullerene is larger. For the systems in which the fullerenes are further away the interaction is minimal. This feature of the DOS behavior can be interpreted according to the characteristic collaborative effects of the aggregates of fullerenes and copolymers described in literature. Therefore, again the synergistic effects of PCBM are very important and it will be very positive to work with real 3D packing to understand them.

However, in general terms,the densities of states of PCBM and the PCBPP systems do not differ significantly, a possible interpretation of this could be that the substitution of the PCBM with a molecule that has a big dipole moment is not affecting the electronic configuration very much. This make it possible to infer that the excitation process will have very much relevance when modeling charge transfer. TD-DFTB in principle would be able to cope with these issues.

If the DOS are the same, which imply that the excitation energies are also the same, and we suppose that such a substitution (p-nitro-N,N-dimethylaniline

has a very high dipole) should produce certain differences, those may lie in the reorganization energies upon excitation. This is subject of further study.

As mentioned in section 2.1 a simulation of a 2D arrangement was performed. A further analysis of it will shed some light on the matter. Very likely the collaborative effects will also enhance the shifts on the density of states.

3.5 Molecular orbitals

The plot of the molecular orbitals (MO) is consistent with the bulk heterojunction scheme presented in the section 1.2.1 . HOMO lays in the copolymer and LUMO in the fullerene part. (HOMO for the copolymer at higher energies that the HOMO of the fullerene derivative, LUMO of the copolymer above the LUMO for the fullerene) (see Figure 3.7 and Figure 3.8).

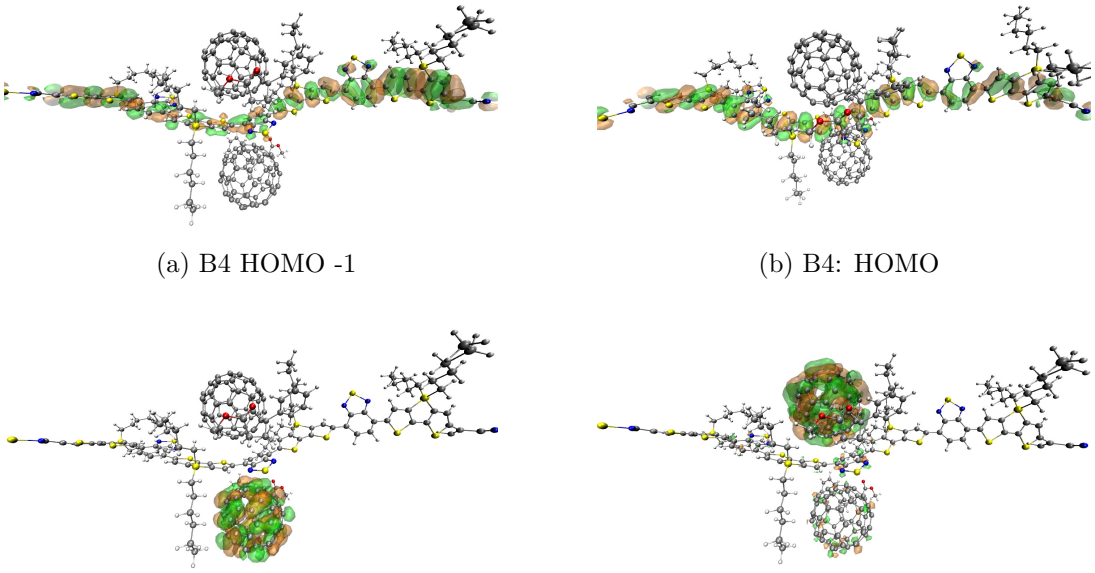

(a) B4 HOMO -1

(b) B4: HOMO

(c) B4: LUMO

(d) B4: LUMO+1

Figure 3.7: MOs of system B4. Iso-surface: 0.003

The behavior of B4 and A4 systems still very much equal when looking to the expected MOs for both of the complexes.

As mentioned above these orbitals were also calculated using DFT (working with ORCA suite [44]), for a cluster geometry (including terminal hydrogens) and they qualitatively resemble the ones produced by DFTB, (see appendix B).

The time needed for this calculation is about quarter of a day using DFT running in 16 processors and for DFTB is about half an hour using 2 processors, this is a clear point in favor of DFTB technique, as equivalent information can be obtain at much less computational cost.

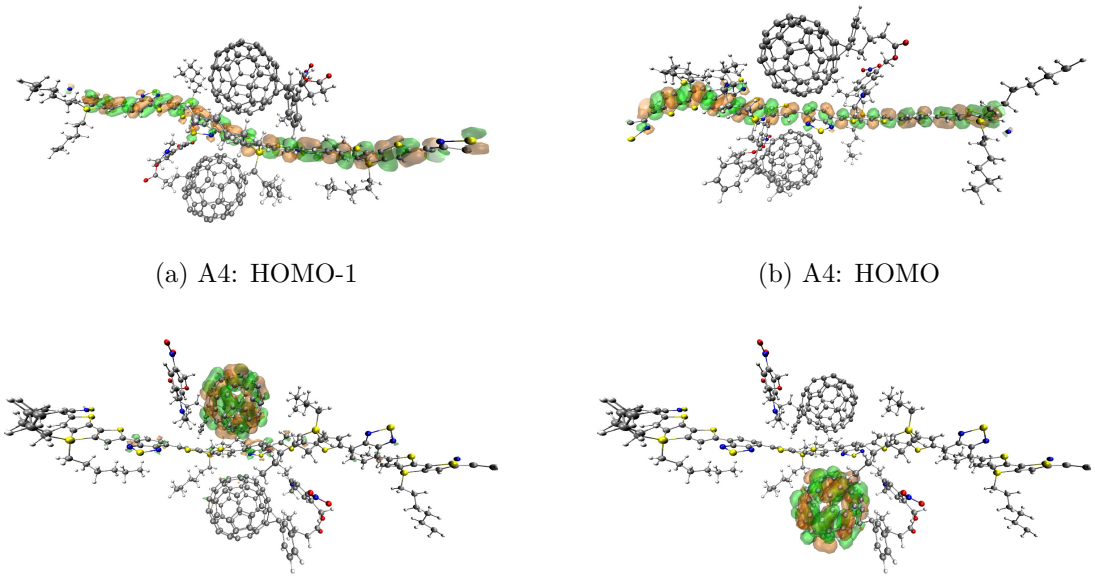

(a) A4: HOMO-1 (b) A4: HOMO

(c) A4: LUMO (d) A4: LUMO+1

Figure 3.8: MOs of system A4. Iso-surface: 0.003

3.6 2D packing

It is presented how after a much longer computational time (c.f. Figure 3.9) equilibrated 2D structures are attained. This is the second step to model BHJ using this level of theory. It may indeed provide a better understanding of the electronic behavior.

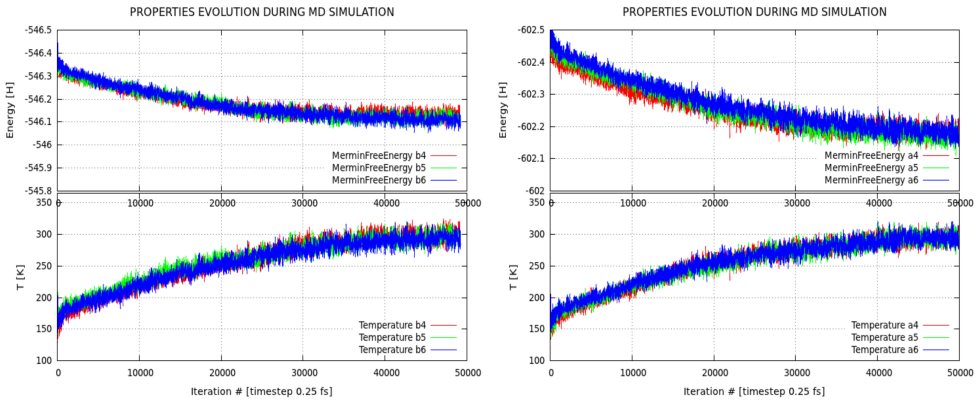

Figure 3.9: MD equilibration for 2D systems

	dist ful-ful	dist to polymer ⊥	placement
A4	6.3Å	2.8Å	benzothiadiazole -
B4	7.4Å	3.5Å	benzothiadiazole -
A5	16.6Å	3.1Å	preferably benzothiadiazole
B5	18.2Å	3.3Å	preferably benzothiadiazole
A6	~8Å	3.1Å	preferably benzothiadiazole
B6	6.8Å	3.2Å	preferably benzothiadiazole

Table 3.5: Morphological distribution of the components of the 2D systems one snapshot only (measured by hand)

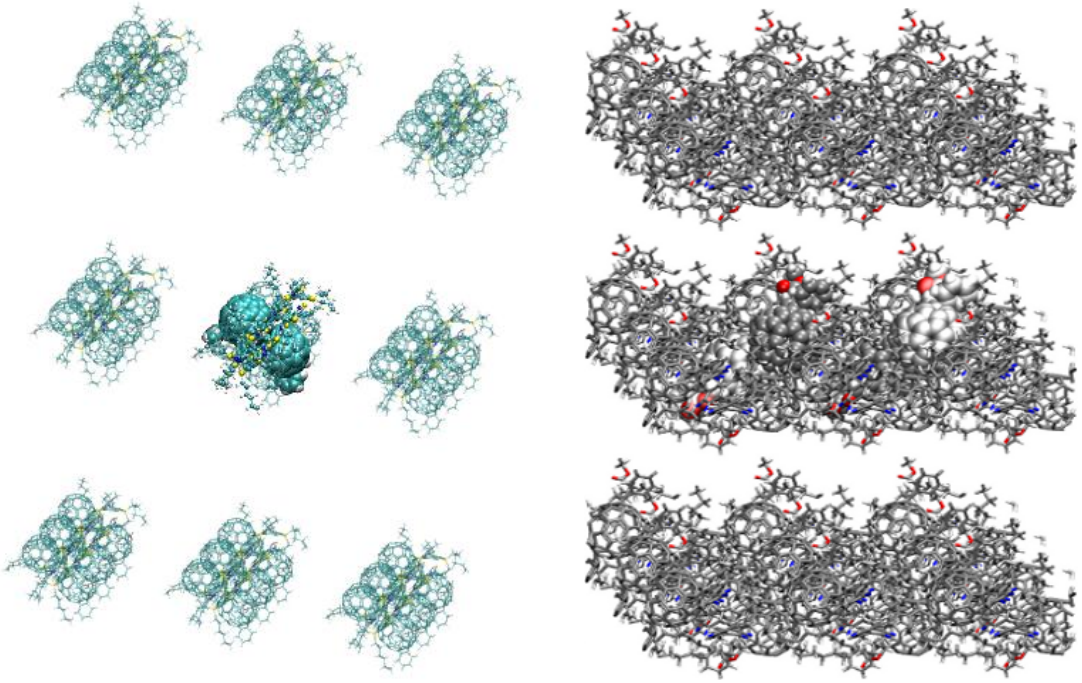

(a) "1D" structure (b) "2D" structure

Figure 3.10: System B4: 1D vs. 2D periodicity comparison

The tighter packing of the 2D case seems to favor a small displacement (~0.1Å) of the fullerene derivatives in both systems toward the polymer chain. The preferred position still the benzothiadiazole. However the buckyballs, in 2D packing, are not directly over the rings but slightly shifted enhancing the interaction fullerene-fullerene.

After looking carefully to the structures data (Table 3.5) it is important to observe that the average distance polymer fullerene for each system is pretty similar to the 1D packing (c.f., Table 3.3), which makes the previous calculations a bit more representative. However the lack of a real statistical analysis does not allow to make too many assumptions.

Chapter 4

Conclusions

In summary, the conceptual and computational framework that had been proposed, is capable to connect (in part) some of the electronic properties with the structure, while looking at the morphological arrangement according to the dynamics.

Llego a mi centro,
a mi álgebra y mi clave,
a mi espejo.
Pronto sabré quién soy.
Jorge Luis Borges

4.1 Main outputs

The stability of systems 4, 5 and 6 containing either PCBM or PCBPP is very similar as it is possible to observe in the graphs within Figure 3.2 or Figure 3.9 respectively. So the initial position of the fullerene derivatives does not affect convergence in for monodimensional systems at last.

The influence of adding a group with high dipole to the PCBM does not affect visibly the mobility nor the other properties investigated for the ground state on these systems. This lead us to the necessity of study both denser packing and excited states in order to reproduce the bigger picture. Mobilities of the chains are quite large and check those in a 3D packing will surely make difference

in how the charge stabilize in excite states calculations.

The orientation of the fullerenes functional groups is very different depending on the snapshot under observation and this might play a role in subsequent reorganization energies upon excitation. In any case, there a clear trend regarding the preference of the buckyballs to be more near to the benzothisdiazole although many times actually, the minimum distance (measured in perpendicular to the polymer plane) will lead us to the region between benzothisdiazole and dithienosilole.

Knowledge of the density of states of a system is equivalent to knowledge of its fundamental equations, from which most thermodynamic quantities can be obtained. Modeling those with accuracy will be a key issue to understand BHJ.

4.2 Outlook

As materials scientists develop a better understanding of the structure-property relationships of organic photovoltaic devices, the efficiencies of organic solar cells will improve and new device architectures will emerge. However, a robust understanding on how morphology affects performance is required in order to apply the full range processing techniques available to organic solar cell fabrication. SCC-DFTB can be effectively used as a bridge between expensive, high-accuracy QM methods and low-accuracy MM force fields. It is proven extensively in literature that SCC-DFTB can reproduce the geometries of many organic molecules and complexes to a large extent.

The investigation of excited states and further study reorganization energies will surely help to go forward in the understanding.

The DFTB tridimensional structure generation will open a new path as this technique is not been used in to study purely organic photovoltaics until this research (as far as I know, DFTB has been used for modeling dye sensitized solar cells).

Using DFTB in GRID might be a good idea, and this would join together the attractive qualities of these two techniques. Any calculations that may be split into many independently parallel parts are suitable for this kind of high performance computing. The distributed and unreliable nature of this resource

makes it unsuitable for closely coupled parallel calculations [45]. In the other hand for calculations like the ones aimed during this research it is very much appropriate, the speed and latency of inter-processor communication will not be a bottleneck. Many geometries are needed, and this might be overcome simply through the addition of grid power.

According to all previous tests, in or out this study, (although our systems are far from realistic), DFTB can be of great help for readily reproduce the MOs of OPV devices.

To conclude, I would like to mention that maybe non-fullerene acceptors can reach higher efficiencies and better stability than it is currently achieved with fullerene-based cells. There are so little differences between A and B whether the molecular formula changes so much that perhaps other acceptors are worth to be consider.

The possibilities are large and fascinating. Computational chemistry will, for sure, play an important role in the multidisciplinary approach needed to tackle this issue.

References

[1] V.S. Arunachalam and E.L. Fleischer. Harnessing materials for energy, 2008.

[2] N.S. Lewis and D.G. Nocera. Powering the planet: Chemical challenges in solar energy utilization. *Proceedings of the National Academy of Sciences*, 103(43):15729–15735, 2006.

[3] Various. Sustainable energy for all, a global action agenda. pathways for concerted action toward sustainable energy for all., April 2012. The Secretary-General's High-Level Group on Sustainable Energy for All.

[4] Writing Team GEA. *Global Energy Assessment (GEA): Toward a Sustainable Future*. Cambridge University press, 2012.

[5] G. Yu, J. Gao, JC. Hummelen, F. Wudl, and AJ. Heeger. Polymer photovoltaic cells: enhanced efficiencies via a network of internal donor-acceptor heterojunctions. *Science-AAAS-Weekly Paper Edition*, 270(5243):1789–1790, 1995.

[6] P. Wurfel. *Physics of Solar Cells: From Principles to New Concepts*. Wiley, 2005.

[7] M. Graetzel. Sensitized solid state heterojunction solar cells. In *European Conference on Hybrid and Organic Solar Cells*, 2006.

[8] B. VanCampen, D. Guidi, and G. Best. Energia solar fotovoltaica para la agricultura y desarrollo rural sostenibles. Online, 2000. FAO - Documento de Trabajo sobre Medio Ambiente y Recursos Naturales, No. 3.

[9] N. Robertson. Optimizing dyes for dye-sensitized solar cells. *Angewandte Chemie International Edition*, 45(15):2338–2345, 2006.

[10] M. Graetzel. Photoelectrochemical cells. *Nature*, 414:338–444, 2001.

[11] B. P. Rand, J. Genoe, P. Heremans, and J. Poortmans. Solar cells utilizing small

molecular weight organic semiconductors. *Progress in Photovoltaics: Research and Applications*, 15(8):659–676, 2007.

[12] L. Dai, D. W. Chang, J-B. Baek, and W. Lu. Carbon nanomaterials: Carbon nanomaterials for advanced energy conversion and storage (small 8/2012). *Small*, 8(8):1122–1122, 2012.

[13] P. Schuster, G. C. Maitland, M. Rigby, E. B. Smith, and W. A. Wakeham. Intermolecular forces - their origin and determination. *Berichte der Bunsengesellschaft fur physikalische Chemie*, 87(3):291–292, 1983.

[14] S. S. Patnaik and R. Pachter. A molecular simulations study of the miscibility in binary mixtures of polymers and low molecular weight molecules. *Polymer*, 43(2):415 – 424, 2002.

[15] P. Mukerji. Polymer-polymer miscibility. *Journal of Polymer Science: Polymer Letters Edition*, 18(8):582–582, 1980.

[16] I. Yarovsky and E. Evans. Computer simulation of structure and properties of crosslinked polymers: application to epoxy resins. *Polymer*, 43(3):963 – 969, 2002. Mattice Special Issue.

[17] P.K. Valavala, T.C. Clancy, G.M. Odegard, and T.S. Gates. Nonlinear multiscale modeling of polymer materials. *International Journal of Solids and Structures*, 44(3-4):1161–1179, 2007.

[18] B. Aradi, B. Hourahine, and Th. Frauenheim. Dftb+, a sparse matrix-based implementation of the dftb method. *The Journal of Physical Chemistry A*, 111(26):5678–5684, 2007. PMID: 17567110.

[19] C. K. Chiang, S. C. Gau, Jr. C. R. Fincher, Y. W. Park, A. G. MacDiarmid, and A. J. Heeger. Polyacetylene, (ch)[sub x]: n-type and p-type doping and compensation. *Applied Physics Letters*, 33(1):18–20, 1978.

[20] C. Piliego, D. Jarzab, G. Gigli, Z. Chen, A. Facchetti, and M. A. Loi. High electron mobility and ambient stability in solution-processed perylene-based organic field-effect transistors. *Advanced Materials*, 21(16):1573–1576, 2009.

[21] C. W. Tang. Two-layer organic photovoltaic cell. *Applied Physics Letters*, 48(2):183–185, 1986.

[22] B.C. Thompson and J.M.J. Frechet. Polymer-fullerene composite solar cells. *Angewandte Chemie International Edition*, 47(1):58–77, 2008.

[23] H. Spanggaard and F. C. Krebs. A brief history of the development of organic and polymeric photovoltaics. *Solar Energy Materials and Solar Cells*, 83:125–146, 2004.

[24] W. Humphrey, A. Dalke, and K. Schulten. VMD – Visual Molecular Dynamics. *Journal of Molecular Graphics*, 14:33–38, 1996.

[25] L. Liao, L. Dai, A. Smith, M. Durstock, J. Lu, J. Ding, and Y. Tao. Photovoltaic-active dithienosilole-containing polymers. *Macromolecules*, 40(26):9406–9412, 2007.

[26] O. Y. Borbulevych, R. D. Clark, A. Romero, L. Tan, M. Y. Antipin, V. N. Nesterov, B. H. Cardelino, C. E. Moore, M. Sanghadasa, and T. V. Timofeeva. Experimental and theoretical study of the structure of n,n-dimethyl-4-nitroaniline derivatives as model compounds for non-linear optical organic materials. *Journal of Molecular Structure*, 604(1):73 – 86, 2002.

[27] W. M. C. Foulkes and R. Haydock. Tight-binding models and density-functional theory. *Phys. Rev. B*, 39:12520–12536, Jun 1989.

[28] M. Elstner, P. Hobza, T. Frauenheim, S. Suhai, and E. Kaxiras. Hydrogen bonding and stacking interactions of nucleic acid base pairs: A density-functional-theory based treatment. *The Journal of Chemical Physics*, 114(12):5149–5155, 2001.

[29] M. Elstner, D. Porezag, G. Jungnickel, J. Elsner, M. Haugk, Th. Frauenheim, S. Suhai, and G. Seifert. Self-consistent-charge density-functional tight-binding method for simulations of complex materials properties. *Phys. Rev. B*, 58:7260–7268, Sep 1998.

[30] Y. Ohta, Y. Okamoto, A. J. Page, S. Irle, and K. Morokuma. Quantum chemical molecular dynamics simulation of single-walled carbon nanotube cap nucleation on an iron particle. *ACS Nano*, 3(11):3413–3420, 2009. PMID: 19827761.

[31] Th. Frauenheim, G. Seifert, M. Elsterner, Z. Hajnal, G. Jungnickel, D. Porezag, S. Suhai, and R. Scholz. A self-consistent charge density-functional based tight-binding method for predictive materials simulations in physics, chemistry and biology. *physica status solidi (b)*, 217(1):41–62, 2000.

[32] C M Goringe, D R Bowler, and E Hernandez. Tight-binding modelling of materials. *Reports on Progress in Physics*, 60(12):1447, 1997.

[33] M. Elstner. The scc-dftb method and its application to biological systems. *Theoretical Chemistry Accounts*, 116:316–325, 2006.

[34] T. A. Niehaus, S. Suhai, F. Della Sala, P. Lugli, M. Elstner, G. Seifert, and Th. Frauenheim. Tight-binding approach to time-dependent density-functional response theory. *Phys. Rev. B*, 63:085108, Feb 2001.

[35] T. A. Niehaus and F. Della Sala. Range separated functionals in the density functional based tight-binding method: Formalism. *physica status solidi (b)*, 249(2):237–244, 2012.

[36] R. M. Wentzcovitch, J. L. Martins, and P. B. Allen. Energy versus free-energy conservation in first-principles molecular dynamics. *Phys. Rev. B*, 45:11372–11374, May 1992.

[37] H. Hoppe, M. Niggemann, C. Winder, J. Kraut, R. Hiesgen, A. Hinsch, D. Meissner, and N.S. Sariciftci. Nanoscale morphology of conjugated polymer/fullerene-based bulk- heterojunction solar cells. *Advanced Functional Materials*, 14(10):1005–1011, 2004.

[38] M. Weinert and J. W. Davenport. Fractional occupations and density-functional energies and forces. *Phys. Rev. B*, 45:13709–13712, Jun 1992.

[39] W. C. Swope, H. C. Andersen, P. H. Berens, and K. R. Wilson. A computer simulation method for the calculation of equilibrium constants for the formation of physical clusters of molecules: Application to small water clusters. *The Journal of Chemical Physics*, 76(1):637–649, 1982.

[40] S. Nose. A unified formulation of the constant temperature molecular dynamics methods. *The Journal of Chemical Physics*, 81(1):511–519, 1984.

[41] W. G. Hoover. Canonical dynamics: Equilibrium phase-space distributions. *Phys. Rev. A*, 31:1695–1697, Mar 1985.

[42] G. J. Martyna, M. L. Klein, and M. Tuckerman. Nos[e-acute]–hoover chains: The canonical ensemble via continuous dynamics. *The Journal of Chemical Physics*, 97(4):2635–2643, 1992.

[43] M. Nolan, S. O'Callaghan, G. Fagas, J. C. Greer, and T. Frauenheim. Silicon nanowire band gap modification. *Nano Letters*, 7(1):34–38, 2007.

[44] F. Neese. The orca program system. *Wiley Interdisciplinary Reviews: Computational Molecular Science*, 2(1):73–78, 2012.

[45] K.Y. Sanbonmatsu and C.-S. Tung. High performance computing in biology: Mul-

timillion atom simulations of nanoscale systems. *Journal of Structural Biology*, 157(3):470–480, 2007. Advances in Molecular Dynamics Simulations.

[46] P. Koskinen and V. Makinen. Density-functional tight-binding for beginners. *Computational Materials Science*, 47(1):237 – 253, 2009.

APPENDIX

Appendix A

Origins of DFTB

Despite having its origin in DFT, one has to bear in mind that DFTB is still a tight-binding method, and should not generally be considered to have the accuracy of full DFT. Absolute transferability can never be achieved, as the fundamental starting point is tightly bound electrons, with interactions ultimately treated perturbatively [46]. Only the formalism for ground-state DFTB will be presented.

A.1 Derivation

Starting from the total energy expression of interacting electron system $E = T + E_{ext} + E_{ee} + E_{II}$, where T is the kinetic energy, E_{ext} the external interaction (including electron–nucleus interactions), E_{ee} the electron–electron interaction, and E_{II} ion–ion interaction energy. Here E_{II} contains terms like the valence of the atom I, and other contributions from the core electrons. In density-functional theory the energy is a functional of the electron density n(r), and for Kohn–Sham system of non-interacting electrons the energy can be written as $E[n(r)] = T_s + E_{ext} + E_H + E_{xc} + E_{II}$, where Ts is the non-interacting kinetic energy, E_H is the Hartree energy, and E_{xc} is the exchange-correlation (xc) energy, hiding all the difficult many-body effects. More explicitly,

$$E[n] = \sum_a f_a \langle \psi_a | \left(-\frac{1}{2}\nabla^2 + V_{\text{ext}} + \frac{1}{2}\int \frac{n(\mathbf{r}')\mathrm{d}^3 r'}{|\mathbf{r}' - \mathbf{r}|} \right) | \psi_a \rangle + E_{xc}[n] + E_{II}$$

where fa∈[0,2] is the occupation of a single-particle state ψ_a with energy ε_a.

Therefore it is possible to consider a system with density $n_0(r)$ that is composed of atomic densities, as if atoms in the system were free and neutral. The density $n_0(r)$ does not minimize the functional $E[n(r)]$, but neighbors the true minimizing density $n_{min}(r)$=$n_0(r)$+$\delta n_0(r)$, where $\delta n_0(r)$ is supposed to be

small. Expanding $E[n]$ at $n_0(r)$ to second order in fluctuation $\delta n(r)$ the energy reads

$$
\begin{aligned}
E[\delta n] \approx & \sum_a f_a \langle \psi_a | -\frac{1}{2}\nabla^2 + V_{\text{ext}} + V_H[n_0] + V_{xc}[n_0] | \psi_a \rangle \\
& + \frac{1}{2} \int \int' \left(\frac{\delta^2 E_{xc}[n_0]}{\delta n \delta n'} + \frac{1}{|\boldsymbol{r} - \boldsymbol{r}'|} \right) \delta n \delta n' - \frac{1}{2} \int V_H[n_0](\boldsymbol{r}) n_0(\boldsymbol{r}) \\
& + E_{xc}[n_0] + E_{II} - \int V_{xc}[n_0](\boldsymbol{r}) n_0(\boldsymbol{r}),
\end{aligned}
$$

That still exact. TB approach implies to substitute the terms of this last equation fitting parameters and making further approximations as it is shown by P. Koskinen and V. Mäkinen, in their didactic paper of 2009 [46].

Appendix B

MOs calculated using DFT

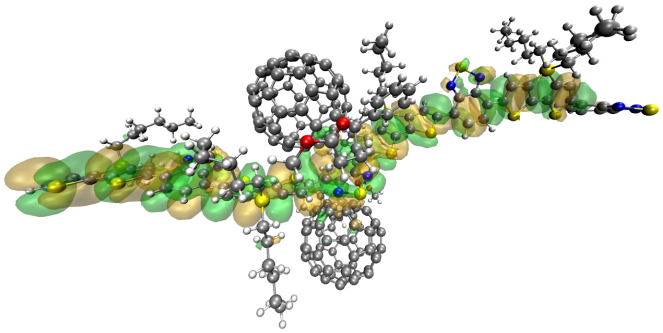

(a) B4 HOMO (isosurface 0.03)

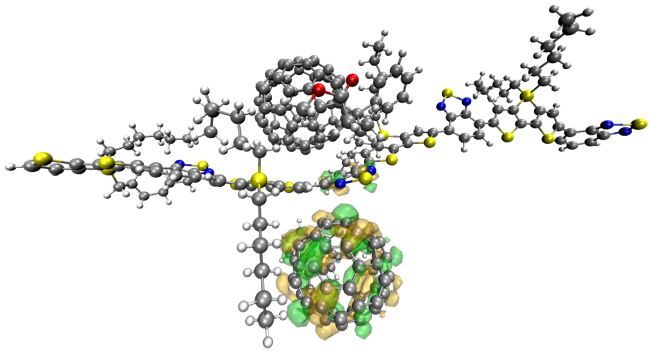

(b) B4 LUMO (isosurface 0.03)

Figure B.1: Molecular orbitals of B4, using B3LYP and 6-31Gd

As it can be evaluated (c.f., Figure 3.8) there are no significant differences with those MOs calculated using DFTB.

Appendix C

Codes used

separate.sh is a script used to extract the copolymer and the fullerenes in order to perform calculations that allow to evaluate the changes upon complex formation.

```
#!/bin/sh

echo running separate.sh

rm copol.* pcbmNMA.*

head -2 geom.gen > head

tail -4 geom.gen > tail

head -250 geom.gen | tail -248 > copol.tmp

tail -220 geom.gen | head -216 > pcbmNMA.tmp

cut -d" " -f2- pcbmNMA.tmp > pcbmNMA.tmp2

cut -d" " -f2- pcbmNMA.tmp2 > pcbmNMA.tmp3

cut -d" " -f2- pcbmNMA.tmp3 > pcbmNMA.tmp4

awk '{print NR,$0}' pcbmNMA.tmp4 > pcbmNMA.tmp5

echo "248 S

C S Si N H" > copol.gen

cat copol.tmp >> copol.gen

cat tail >> copol.gen

echo "216 S

C N H O" > pcbmNMA.gen

cat pcbmNMA.tmp5 >> pcbmNMA.gen

cat tail >> pcbmNMA.gen
```

```
 sed "s/ 4 / 2 /g" -i pcbmNMA.gen

 sed "s/ 5 / 3 /g" -i pcbmNMA.gen

 sed "s/ 6 / 4 /g" -i pcbmNMA.gen

rm *.tm*

cp pcbmNMA.gen PCBM/geom.gen cp copol.gen COPOLYM/geom.gen

cp ~/data/Te100/a4/MD/DOS/k4/PCBMnma/dftb_in.hsd PCBM/dftb_in.hsd

cp ~/data/Te100/a4/MD/DOS/k4/COPOLYM/dftb_in.hsd COPOLYM/dftb_in.hsd

echo ‘‘done’’
```

With the **ContinueMDrun.flv** it is possible to concatenate sorter MD runs assuring a coherent final trajectory minimizing the risk to lose data if a calculation crash half way through.

```
#!/bin/sh

# # Submit a DFTB job to a batch queue on falcon

# # $1 -- name of queue # $2 -- name of input file # $3 -- wall time (hours)

# # First check if the queue exists #

if [ $# -ne 3 ]

then

echo "Usage:  $0 queue jobname walltime (hh:mm:ss)"

exit 1 fi

queue=$1

checkedqueue=‘/usr/local/bin/queuelookup $1|grep Sorry‘

if [ "$checkedqueue" != "" ]

then

/usr/local/bin/queuelookup $1

echo "Resubmit to valid queue"

/usr/local/bin/qstat -Q

exit 2 fi

# # Check if the submission is for a Xeon queue #

checkedqueue=‘/usr/local/bin/queuelookup_xeon $1|grep xeon‘

if [ "$checkedqueue" = "" ]
```

```
then processor_type=xeon

else # Check if the submission is for an opteron queue

checkedqueue=‘/usr/local/bin/queuelookup_opteron $1|grep opteron‘

if [ "$checkedqueue" = "" ]

then processor_type=opteron

else #Neither xeon nor opteron

processor_type=common fi fi

# Declare number of processors

NPROC=2

# Start creating the input file

cat <<END >>$2.job

#PBS -S /bin/sh

#PBS -A $USER

#PBS -k eo

#PBS -q $1

#PBS -N $2

#PBS -l mem=2gb

END

# Check whether a time specification has been inserted

cat <<END >>$2.job

#PBS -l nodes=1:ppn=$NPROC

#PBS -l walltime=$3

END

cat <<END >>$2.job

traj_dir=\‘pwd | sed -e "s/\//@/g" | cut -d ’@’ -f 5-\‘

PATH="\$PATH:/home/morokuma3/page/src_dev2:/usr/local/bin:/home/morokuma3/rpg/bin"
; export PATH

dir="/scratch/\$\$" ; export dir

OMP_NUM_THREADS=$NPROC ; export OMP_NUM_THREADS

if [ !  -d \$dir ]
```

```
then mkdir \$dir

fi

# set irun, iend-----------------------------------

irun=19 iend=25

#-------------------------------------------------

echo 'start' > \$PBS_O_WORKDIR/run.log

date >> \$PBS_O_WORKDIR/run.log

while [ "\$irun" -le "\$iend" ]

do

run_dir=\$PBS_O_WORKDIR/run\${irun}

cd \$dir

cp \$run_dir/dftb_in.hsd \$dir/dftb_in.hsd

gen=\`sed -n "/Geometry/,+1 p" dftb_in.hsd | tail -n1 | sed "s/[<,\ ,\"]//g"\`

cp \$run_dir/\$gen \$dir

out=\`sed -n "/outputprefix/p" dftb_in.hsd | sed 's/outputprefix//g' | sed 's/[\
,=,\"]//g'\`

natom=\`head -n1 \$gen | sed 's/[s,S,c,C,\ ]//g'\`

if [ -f \$run_dir/VELOC.DAT ]

then

cp \$run_dir/VELOC.DAT \$dir

fi

date >> \$run_dir/run.out

/source/dftb+_1.1_src.nhc/prg_dftb/_obj_x86_64-linux-ifort/dftb+ < dftb_in.hsd >>
\$run_dir/run.out

date >> \$run_dir/run.out

# # check for strange segmentation fault

# behaviour observed on falcon.  if the

# correct number of MD steps have not

# been taken, exit the job

nstep=\`grep 'Geometry step' \$run_dir/run.out | tail -n1 | sed 's/.\{18\}//g'\`

if [ \$nstep -ne 1000 ]
```

```
then
echo "run \$irun:  Geometry steps = \$nstep ....  Exiting" exit 0
fi
#-----------------------------------------
mv \$dir/* \$run_dir
rm \$run_dir/dftb_pin.hsd
# # advance
#
cd \$PBS_O_WORKDIR
jrun=\‘expr \$irun + 1\‘
/home/morokuma4/rpg/bin/dftb+cp run\${irun} run\${jrun}
# /home/morokuma3/haibei/bin/dftb+cp run\${irun} run\${jrun}
irun=\‘expr \$irun + 1\‘
done
echo ’end’ >> \$PBS_O_WORKDIR/run.log
date >> \$PBS_O_WORKDIR/run.log
echo ’ ’
rm -fr \$dir
cd \$PBS_O_WORKDIR
END
# Now submit it.  qsub $2.job rm -f $2.job
# Wait a short time and exit sleep 1
```